Check for updates

ChemElectroChem

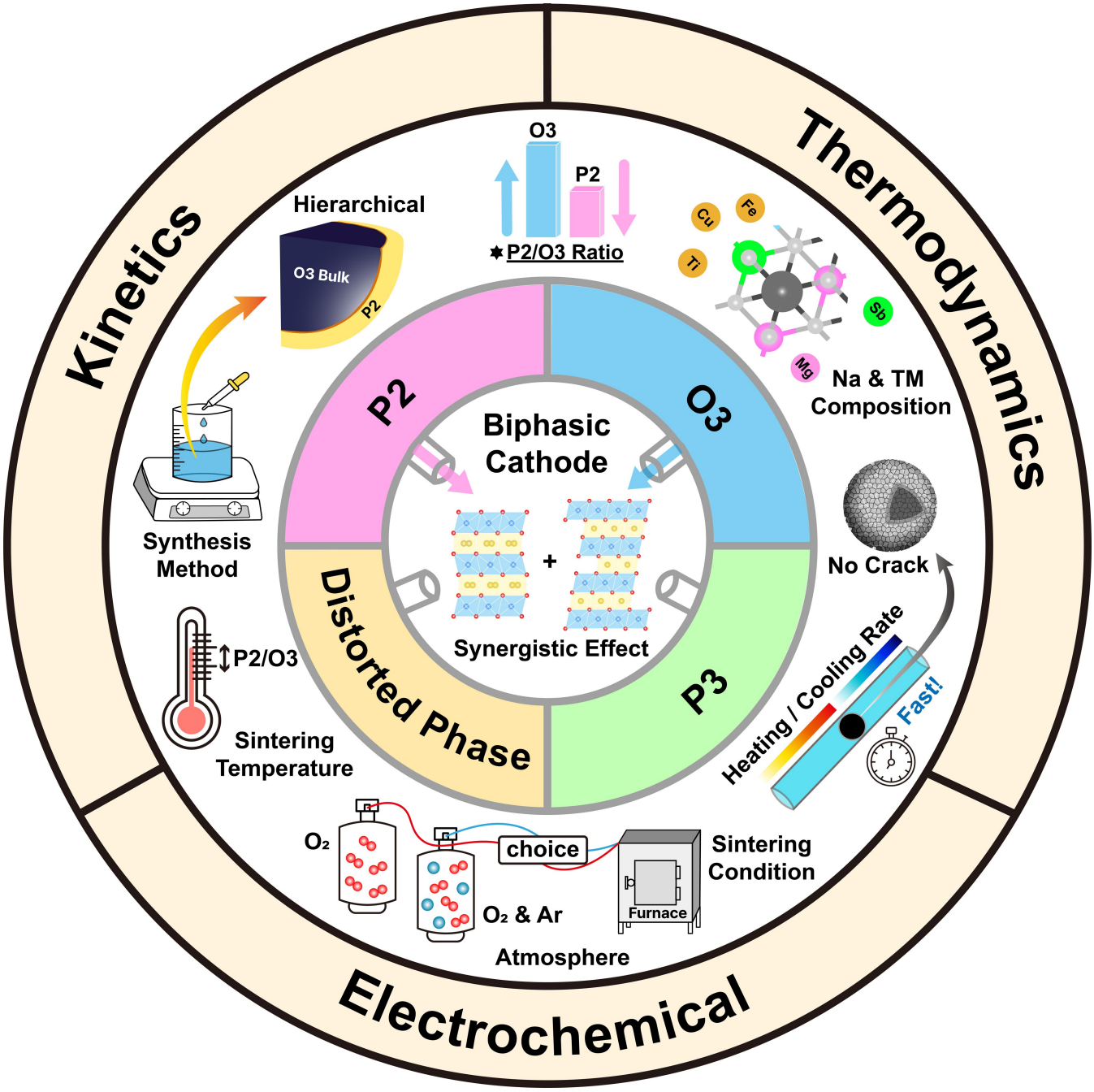
Review
doi.org/10.1002/celc.202400657

Chemistry Europe
European Chemical Societies Publishing

www.chemelectrochem.org

Enhancing Sodium Ion Battery Performance through Biphasic Layered Oxide Cathodes

Seung-Jun Kang,[a] Sung-Joon Park,[a] Kwan Woo Nam,*[c] and Seung-Ho Yu*[a, b]



© 2025 The Authors. ChemElectroChem published by Wiley-VCH GmbH

21960216, 2025, 7, Downloaded from https://chemistry-europe.onlinelibrary.wiley.com/doi/10.1002/celc.202400657 by Ewha Womans University Library, Wiley Online Library on [10/08/2025]. See the Terms and Conditions (https://onlinelibrary.wiley.com/terms-and-conditions) on Wiley Online Library for rules of use; OA articles are governed by the applicable Creative Commons License

Biphasic layered cathodes represent a strategic advancement in overcoming the inherent limitations of single-phase materials by synergistically integrating distinct phase characteristics. Among these, the P2/O3 biphasic cathode stands out due to its integration of the rapid diffusion kinetics of the P2 phase with the high capacity of the O3 phase, resulting in superior battery performance. Given the critical role of phase ratio in determining the performance of biphasic cathodes, this work systematically examines the influence of synthesis methods, sintering temperatures, and sodium and dopant compositions on phase modulation. A comprehensive analysis of the kinetic and thermodynamic properties of the P2/O3 cathode is conducted, with findings correlated to electrochemical data to elucidate how thermodynamic stability and efficient diffusion kinetics contribute to enhanced functionality. Finally, a brief overview of other biphasic cathodes is provided, comparing their distinctive properties relative to those of the P2/O3 system.

1. Introduction

Lithium-ion batteries (LIBs) have played a crucial role as an energy source for various essential devices in our lives, particularly contributing to the rapid growth of the electric vehicle market.[1] However, as the electric vehicle market continues to expand, the demand for LIBs has increased, and the depletion of metal resources, including lithium, is driving up costs. In the long term, this trend may hinder the potential application of LIBs in large-scale energy storage and could lead to market stagnation.

To address the limitations of LIBs, extensive research is being conducted on next-generation batteries such as sodium-ion batteries (SIBs), lithium metal batteries, and all-solid-state batteries. Among these, SIBs offer significant cost advantages over LIBs. This is partly due to the lower cost of cathode materials and the potential to replace the expensive copper (Cu) foils used in anode current collectors with cheaper aluminum (Al) foils, leading to an overall cost reduction of at least 10% compared to LIBs.[2] Moreover, the intercalation chemistry of sodium is quite similar to that of lithium, enabling the use of similar compounds for both systems.

However, Na^+ ions (1.02 Å) are larger than Li^+ ions (0.76 Å), which impacts phase stability, transport properties, and interphase formation. Additionally, sodium is heavier than lithium (23 g mol^{-1} vs. 6.9 g mol^{-1}) and has a higher standard electrode potential (-2.71 V vs. SHE compared to -3.02 V for lithium), resulting in lower energy density for SIBs.[3] Other challenges, such as poor stability, low ionic conductivity, and capacity degradation due to structural instability at high voltages, remain key issues for further improvement in SIB system.

Given the importance of cathodes in enhancing the energy density of SIBs to levels comparable with those of LIBs, various types of cathode materials have been systematically investigated, including polyanionic compounds, Prussian blue analogs, layered oxides, and organic-based materials. Among them, transition metal (TM)-based layered oxides (Na_xTMO_2, where TM=Fe, Mn, Ni, Co, etc.) have emerged as the most promising candidates for SIB cathodes due to their superior specific capacity, relatively simple preparation methods, and reference to the successful application of $LiTMO_2$ in LIB systems.[4]

According to previous studies, based on the Na sites (prismatic or octahedral) and the stacking sequence of the O layers (ABBA or ABCABC), Na_xTMO_2 generally forms P2 (Na/TM $<$ 0.8, prismatic, ABBA) or O3 (Na/TM $>$ 0.8, octahedral, ABCABC) structures.[5–8] P2-type oxides typically exhibit higher Na-ion conductivity and better structural stability compared to their O3 counterparts, contributing to improved power density and cycling performance.[9] However, both P2 and O3 Na_xTMO_2 structures undergo significant and irreversible phase transitions in high-voltage regions, leading to a loss of structural stability and reduced cycling performance.[10–12] In contrast, biphasic materials can combine the advantages of both structures, offering multifunctional benefits and significantly enhancing electrochemical performance compared to single-phase materials.[13–15] In addition to P2/O3 biphasic oxides, Na_xTMO_2 cathode materials with P2/P3, P3/O3, P2/O′3, O3/spinel, P2/O3/O1, P2/O′3/spinel binary or ternary phases have been reported recently.[16–19, 84, 85]

In this review, we examine the synthesis and design of the P2/O3 biphasic cathode, a representative biphasic material, and aim to analyze in detail why it delivers superior battery performance compared to single-phase cathodes by examining differences in kinetics, thermodynamics, and electrochemical characteristics through various analytical methods. Additionally, we compare the P2/O3 biphasic cathode with other biphasic systems such as P2/P3, P3/O3, and P2/O′3, assessing which demonstrates better performance, and suggest prospects and directions for biphasic cathode research.

[a] S.-J. Kang, S.-J. Park, S.-H. Yu
Department of Chemical and Biological Engineering, Korea University, 145 Anam-ro, Seongbuk-gu, 02841 Seoul, Republic of Korea
E-mail: seunghoyu@korea.ac.kr

[b] S.-H. Yu
Department of Battery-Smart Factory, Korea University, 145 Anam-ro, Seongbuk-gu, 02841 Seoul, Republic of Korea
E-mail: seunghoyu@korea.ac.kr

[c] K. W. Nam
Department Chemical Engineering and Materials Science, and Graduate Program in System Health Science and Engineering, Ewha Womans University, Seoul 03760, Republic of Korea
E-mail: kwanwoo@ewha.ac.kr

© 2025 The Authors. ChemElectroChem published by Wiley-VCH GmbH. This is an open access article under the terms of the Creative Commons Attribution License, which permits use, distribution and reproduction in any medium, provided the original work is properly cited.

2. P2/O3 Biphasic Cathode

2.1. P2/O3 Composite Synthesis

The formation mechanisms of the biphasic layered structure have been scarcely discussed so far, and the mechanisms during sodiation/desodiation within this structure remain unclear. Synthesizing P2/O3 biphasic cathode materials presents additional complexity compared to single-phase materials. As optimal phase formation is essential for achieving high battery performance, a comprehensive understanding of these underlying mechanisms is crucial. This synthesis process is governed by three key controllable factors: the synthesis method, the sodium and dopant composition, and the sintering condition. In the following section, we provide a detailed overview of how each of these factors influences phase formation.

When synthesizing P2/O3 biphasic cathode materials, different synthesis processes are used to control phase formation and their own unique structures. Structural modification strategies have long been employed to enhance performance in both LIBs and SIBs.[89, 90] For example, Jianling et al. proposed a high-performance lithium-rich cathode featuring a dual gradient of aluminum and oxygen vacancies, as well as a heterogeneous structure, achieved through aluminum solution treatment.[25] Typically, the solid-state method is commonly employed, but by utilizing a coating process, a hierarchical structure can be formed where the surface possesses a P2 phase and the bulk interior an O3 phase.[32, 88] This structure is utilized to overcome the poor air stability of O3-type materials, which generally react with moist air to form NaOH and Na_2CO_3.[26] After surface coating through a wet chemistry process followed by high-temperature calcination, a material with a heterostructure consisting of a P2 surface and an O3 bulk is formed, as illustrated in Figure 1a. Consequently, the enhanced Na storage performance of the heterostructured cathode is related to the synergistic effect of the biphasic structure, in which the O3 phase core provides a sufficient initial Na reservoir, while the P2-type structure acts as a robust protective layer.[20] Raghvendra et al. synthesized biphasic materials by using both the solid-state method (Bi doping) and wet chemical coating (Bi_2O_3 coating).[27] The former enlarges the interlayer spacing, while the latter provides ionic conducting channels and protects the particles from electrolyte contact.

The content of various transition metals and sodium is one of the key factors determining the phase of cathode materials in SIBs. While layered oxide cathodes (Na_xTMO_2) generally form a P2 phase at low sodium content and an O3 phase at high sodium content, exceptions exist, underscoring the need for a more precise system to predict phase formation. For P2/O3 biphasic cathodes, especially in materials with complex compositions, it is often challenging to predict the structure and the phase ratio between the two phases. Therefore, recent studies have introduced concepts such as "cationic potential" and "radial potential," which can be used to predict the key interactions and stacking sequences of layered materials. This approach is crucial in the pursuit of forming the desired phase. Figure 1b provides a schematic representation of the predicted phase formation for various cathode materials based on their calculated cationic potentials. In general, the P2/O3 biphasic cathode is observed to form near the boundary($y = 0.4065x + 1.572$) between regions where P2 and O3 phases are typically formed. The cationic potential is calculated using the following equation:

$$\Phi_{cation} = \frac{\overline{\Phi_{TM}}\ \overline{\Phi_{Na}}}{\overline{\Phi_O}}$$

In layered oxides like $NaTMO_2$, the average ionic potential of the transition metals ($\overline{\Phi_{TM}}$) plays a significant role, where the content of TM, charge number, and radius are crucial factors. As the cationic potential increases, the stronger TM electron cloud extension and interlayer electrostatic repulsion lead to the



Seung-Jun Kang received his B.S (2024) degree in Chemical and Biological Engineering from Korea University. He is currently a Ph.D. candidate in Chemical and Biological Engineering at Korea University. His research is focused on cathode material designs for Sodium-ion batteries and anode material designs for Litium-ion batteries.



Kwan Woo Nam is currently an assistant professor in the Department of Chemical Engineering and Materials Science at Ewha Womans University. His research is mainly focused on the development of emerging materials and analyzing the reaction mechanisms for next-generation secondary batteries.



Sung-Joon Park obtained his B.S. (2021) degree in Chemical and Biological Engineering from Korea University. He is currently a Ph.D. candidate in Chemical and Biological Engineering at Korea University. His research is focused on cathode material designs for alkali metal-based secondary batteries.



Seung-Ho Yu is an associate professor in the Department of Chemical and Biological Engineering at Korea University and concurrently holds a position as a professor in the Department of Battery-Smart Factory at Korea University. His current research focuses on material design and revealing reaction mechanisms for (post) Li-ion batteries.

© 2025 The Authors. ChemElectroChem published by Wiley-VCH GmbH

21960216, 2025, 7, Downloaded from https://chemistry-europe.onlinelibrary.wiley.com/doi/10.1002/celc.202400657 by Ewha Womans University Library, Wiley Online Library on [10/08/2025]. See the Terms and Conditions (https://onlinelibrary.wiley.com/terms-and-conditions) on Wiley Online Library for rules of use; OA articles are governed by the applicable Creative Commons License

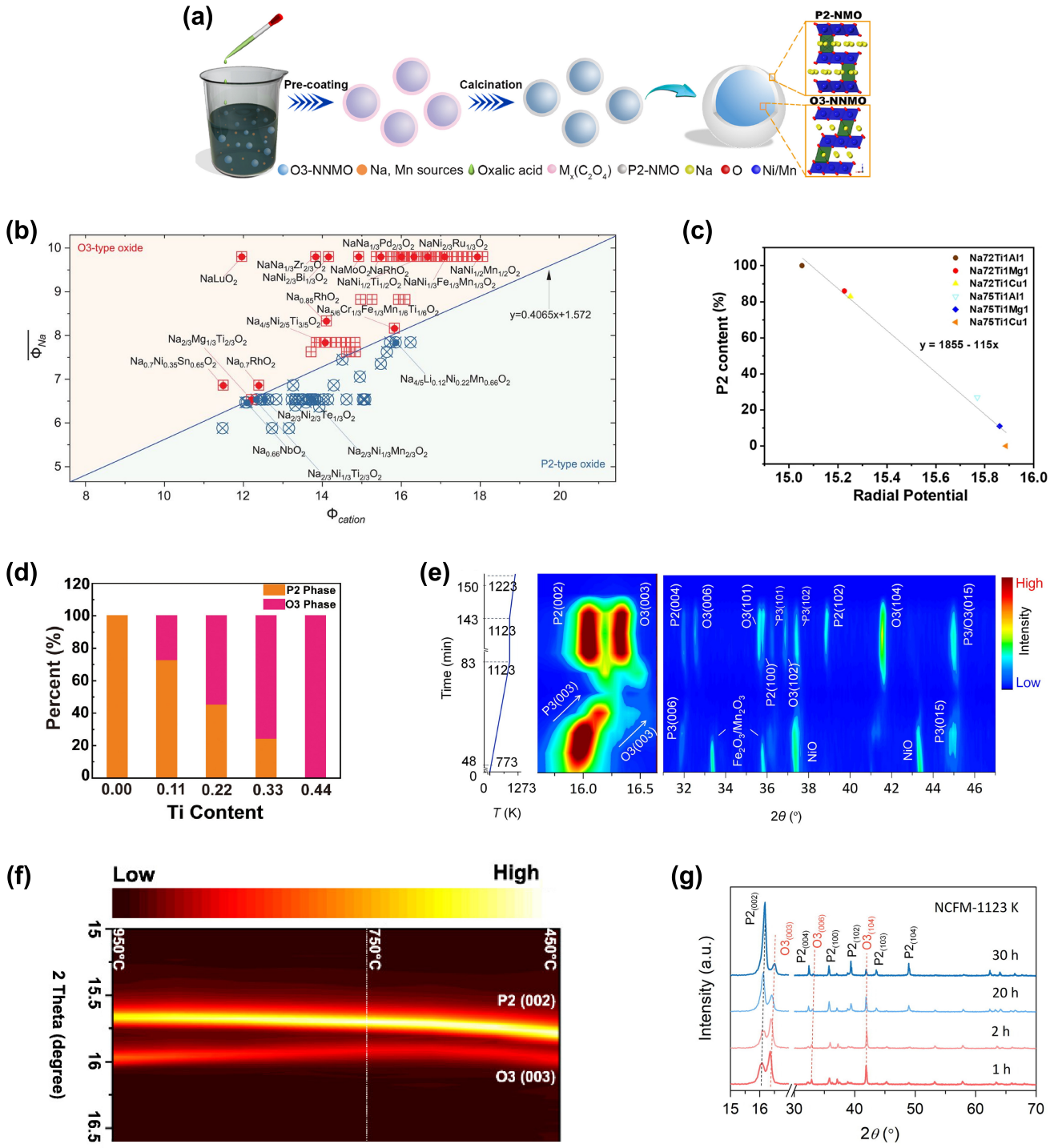


Figure 1. (a) Schematic of the synthesis of the O3/P2 heterostructure cathode material. Reproduced with permission from ref [20]. Copyright 2022, Elsevier. (b) Cationic potential of representative P2- and O3-type Na-ion layered oxides. Reproduced with permission from ref [21]. Copyright 2022, Elsevier. (c) Plot of P2 content against radial potential. Reproduced with permission from ref [22]. Copyright 2023, Springer Nature. (d) Phase transition P2 to O3 with increasing Ti content. Reproduced with permission from ref [23]. Copyright 2022, Elsevier. (e) Phase evolution during solid-state synthesis of P2/O3 biphasic material monitored by in situ XRD. Reproduced with permission from ref [24]. Copyright 2022, Elsevier. (f) P2(002) and O3(003) peak intensity variations during the cooling process monitored by XRD patterns. Reproduced with permission from ref [88]. Copyright 2024, American Chemical Society. (g) Phase transition with different quenching time after sintering. Reproduced with permission from ref [24]. Copyright 2022, Elsevier.

formation of the P2-type structure, with more covalent TM–O bonds and an increased $d_{(O\text{-}Na\text{-}O)}$ distance.[21] In addition to the cationic potential, Maughan et al. expanded and refined the new concept of "radial potential" to design biphasic O3/P2 hybrid materials and compare the use of ionic radius and cationic potential as predictors.[22] The radial potential is defined by the following equation:

© 2025 The Authors. ChemElectroChem published by Wiley-VCH GmbH

21960216, 2025, 7, Downloaded from https://chemistry-europe.onlinelibrary.wiley.com/doi/10.1002/celc.202400657 by Ewha Womans University Library, Wiley Online Library on [10/08/2025]. See the Terms and Conditions (https://onlinelibrary.wiley.com/terms-and-conditions) on Wiley Online Library for rules of use; OA articles are governed by the applicable Creative Commons License

$$\text{Radial Potential} = \frac{\text{Average TM radius} * \text{Weighted Na potential}}{\text{Weighted oxygen potential}}$$

This concept focuses on using the average ionic radius of the TM layer to predict how small changes in the composition of the Na and TM layers influence the O3/P2 ratio, allowing for control over the P2 content. As shown in Figure 1c, materials with lower radial potential tend to form a higher proportion of the P2 phase. An example of applying these two concepts can be seen in Figure 1d. In Ni- and Mn-based cathode materials, replacing Mn with Ti and increasing the Ti content leads to a higher proportion of the O3 phase.[91] This is because Ti has a lower average ionic potential compared to Mn, leading to increased formation of the O3 phase with higher Ti content. The effects of various doping elements will be discussed in detail in the following section. Not only titanium but also Li and Cu promote the formation of the O3 phase, while B contributes to P2 phase formation.[28–31] Therefore, careful selection of dopants is crucial for controlling phase formation.

Lastly, phase formation can be controlled by adjusting the sintering conditions, including temperature, heating/cooling rate, and atmosphere. As shown in Figure 1e, NCFM materials begin forming the P3 phase at 773 K. With increasing temperature, the O3 phase emerges, leading to the coexistence of both phases at 1073 K. At 1123 K, the P2 phase starts to form, and after maintaining the material at 1123 K for 60 minutes, the P2/O3 phases can be observed. Pengfei et al. investigated the formation of the P2/O3 biphasic structure in the high-entropy $Na_{0.7}Mn_{0.4}Ni_{0.3}Cu_{0.1}Fe_{0.1}Ti_{0.1}O_{1.95}F_{0.1}$ cathode material during the sintering process by adjusting the temperature.[45] Unlike the NCFM biphasic cathode, phase formation in this case followed the sequence P3 - P2 - O3, with the P2/O3 biphasic structure forming between 750 °C and 900 °C. Interestingly, as the temperature rose above 900 °C, the proportion of the P2 phase increased again. These findings highlight the importance of understanding the specific temperature ranges and phase transformation profiles for each material during the synthesis process.

While the heating process dictates the initiation and transition of various phases, the cooling process, particularly the cooling rate, plays a decisive role in the final phase composition. Although detailed conditions are often not disclosed for biphasic materials in the literature, it is generally observed that slower cooling rates favor the formation of a single phase, whereas faster cooling rates tend to result in the coexistence of P2 and O3 phases within the material. As illustrated in Figure 1f, during a natural cooling process involving a rapid temperature drop from 950 °C to 450 °C, the P2 peak intensity increases, whereas the O3 peak intensity decreases. This indicates a continuous phase transformation within the material, leading to a sharp increase in the proportion of the P2 phase, from 46.0% to 63.6%. Furthermore, extending the quenching time with much slower rate, consistent with Figure 1f, increases the proportion of the P2 phase in the P2/O3 biphasic cathode and, when prolonged excessively, leads to the formation of an extreme P2/O3 ratio (Figure 1g).

Atmospheric control during the synthesis process provides yet another pathway for optimizing phase formation. Yihang et al. demonstrated that by adjusting the duration or rate of Ar flushing to balance the Ar and O_2 atmosphere, the proportion of the P2 phase within the material can be effectively controlled.[87] This approach not only enhances the stability of the desired phase but also improves the reversibility and kinetics of the anionic redox process. Overall, these findings highlight the intricate interplay of temperature, cooling rate, and atmosphere in determining phase composition. By carefully optimizing these parameters, it is possible to tailor the structural and electrochemical properties of biphasic cathode materials to meet specific performance requirements.

2.2. Thermodynamics

Understanding the thermodynamic properties of cathode materials is crucial, as these characteristics directly influence structural evolution and electrochemical performance.[36] During the charge and discharge process, sodium ions migrate within cathode materials, leading to structural changes as the material forms the most thermodynamically stable phase. However, when charged to high voltages, typical single-phase sodium layered oxides often undergo irreversible phase transitions, such as $O3_{hex.}$–$O3'_{mon.}$–$P3_{hex.}$–$P3'_{mon.}$–$P3''_{hex}$, and frequently fail to recover their original phase during discharge.[37, 38]

In contrast, P2/O3 biphasic cathodes are known to reversibly recover phases by forming intermediate phases such as OP4 and OP2. The P2/O3 biphasic cathode may undergo distinct phase transitions influenced by factors such as the composition and content of sodium and transition metals, and the applied voltage range during cycling, all of which affect the material's phase transition mechanism. Lianzheng et al. demonstrated that the distinct phase transitions in P2/O3 biphasic materials, along with the suppression of volumetric changes and manganese dissolution compared to single-phase counterparts, are primarily attributed to the "interlocking effect" at the P2/O3 phase boundary (Figure 2a). This effect implies that the P2 phase acts as a structural pillar, stabilizing the framework and mitigating stress during the O3–P3 phase transition. Therefore, achieving an optimal balance of P2 and O3 phases is crucial for ensuring stable performance, as it enables the material to maintain its structural integrity during phase transitions. However, the ideal P2/O3 ratio varies depending on the material, and no universal standard has been established to date. As shown in Table 1, materials with various P2/O3 ratios have been extensively studied, highlighting the diversity in potential phase compositions. Moreover, even for materials with the same overall composition, significant performance variations can arise depending on the P2/O3 ratio. To mitigate such issues and avoid performance degradation, once the material composition is determined, optimizing the sintering conditions – such as temperature, atmosphere, and cooling rate – can enable precise control over the P2/O3 ratio, as discussed in Section 2.1.

© 2025 The Authors. ChemElectroChem published by Wiley-VCH GmbH

21960216, 2025, 7, Downloaded from https://chemistry-europe.onlinelibrary.wiley.com/doi/10.1002/celc.202400657 by Ewha Womans University Library, Wiley Online Library on [10/08/2025]. See the Terms and Conditions (https://onlinelibrary.wiley.com/terms-and-conditions) on Wiley Online Library for rules of use; OA articles are governed by the applicable Creative Commons License

21960216, 2025, 7, Downloaded from https://chemistry-europe.onlinelibrary.wiley.com/doi/10.1002/celc.202400657 by Ewha Womans University Library, Wiley Online Library on [10/08/2025]. See the Terms and Conditions (https://onlinelibrary.wiley.com/terms-and-conditions) on Wiley Online Library for rules of use; OA articles are governed by the applicable Creative Commons License

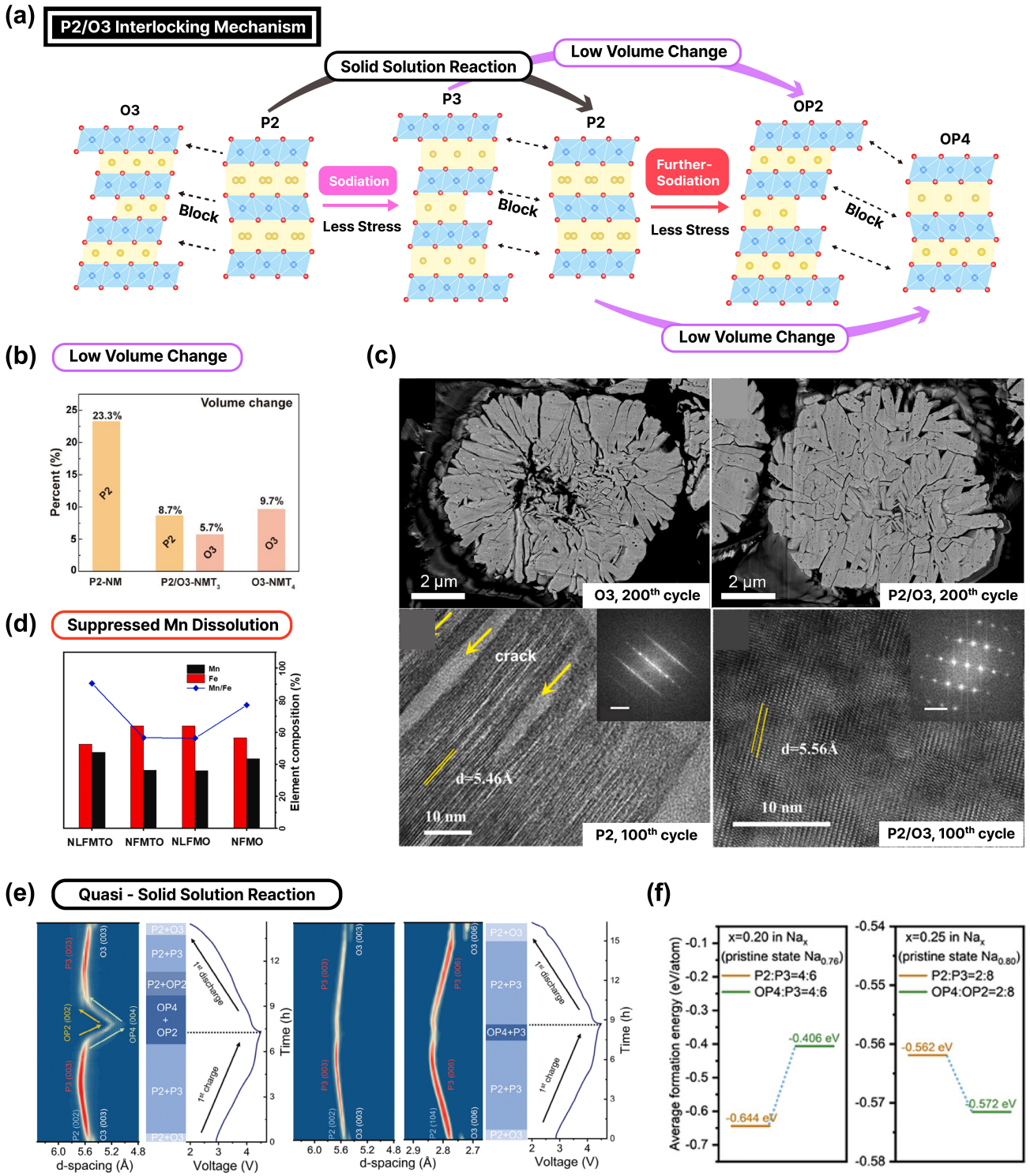


Figure 2. (a) Interlocking mechanism of P2/O3 biphasic cathode during the charging. Reproduced with permission from ref [23]. Copyright 2022, Elsevier. (b) Volume change of Ti doped P2/O3 biphasic cathode compared with single phase materials after the charging process. Reproduced with permission from ref [23]. Copyright 2022, Elsevier. (c) SEM & TEM images of P2/O3 biphasic cathode(right) and single-phase cathode(left) after long cycles. Reproduced with permission from ref [20], [34]. Copyright 2021 & 2022, Elsevier. (d) The Fe/Mn relative contents and the deduced Mn/Fe ratio detected by XRF test after 100 cycles. Reproduced with permission from ref [34]. Copyright 2021, Elsevier. (e) Phase transition of biphasic cathodes with varying P2/O3 ratios monitored by in-situ XRD contour map. Reproduced with permission from ref [33]. Copyright 2024, Wiley-VCH. (f) The average formation energy of different phases for P2/O3 biphasic cathodes. Reproduced with permission from ref [33]. Copyright 2024, Wiley-VCH.

Optimized phase ratios not only enhance the material's ability to efficiently manage sodium extraction but also contribute to mitigating structural instabilities. As sodium ions are continuously extracted, the P2 and P3 structures mutually

© 2025 The Authors. ChemElectroChem published by Wiley-VCH GmbH

21960216, 2025, 7, Downloaded from https://chemistry-europe.onlinelibrary.wiley.com/doi/10.1002/celc.202400657 by Ewha Womans University Library, Wiley Online Library on [10/08/2025]. See the Terms and Conditions (https://onlinelibrary.wiley.com/terms-and-conditions) on Wiley Online Library for rules of use; OA articles are governed by the applicable Creative Commons License

Table 1. Electrochemical properties of the P2/O3 biphasic layered oxide cathode for SIBs.

Cathode materials	P2/O3 ratio	Reversible capacity	Capacity retention	Ref.
P2/O3-$Na_{7/9}Ni_{2/9}Mn_{4/9}Fe_{1/9}Mg_{1/9}Li_{1/9}O_2$	P2(47.6%), O3(52.4%)	170.5 mAh g^{-1}/0.1 C/2.0–4.4 V	87.3%/100cycles/1 C	[46]
P2/O3-$Na_{1.01}Ni_{0.49}Mn_{0.53}B_{0.019}O_2$	P2(24.53%), O3(75.47%)	119.4 mAh g^{-1}/0.1 C/2.0–4.0 V	85.2%/1000cycles/5 C	[38]
P2/O3-$Na_{0.85}Ni_{0.34}Mn_{0.33}Ti_{0.33}O_2$	P2(24.8%), O3(75.2%)	126.6 mAh g^{-1}/0.1 C/2.2–4.4 V	80.6%/200cycles/1 C	[23]
P2/O3-$Na_{0.7}Ni_{0.2}Cu_{0.1}Fe_{0.2}Mn_{0.5}O_{2-\delta}$	P2(55.9%), O3(39.3%)	115 mAh g^{-1}/12 mA g^{-1}/2.4–4.2 V	84%/500 cycles/240 mA g^{-1}	[24]
P2/O3-$Na_{0.7}Mn_{0.4}Ni_{0.3}Cu_{0.1}Fe_{0.1}Ti_{0.1}O_{1.95}F_{0.1}$	P2(23%), O3(77%)	133.7 mAh g^{-1}/20 mA g^{-1}/2.0–4.3 V	88.9%/200 cycles/200 mA g^{-1}	[45]
P2/O3-$Na_{0.76}Cu_{0.1}Co_{0.1}Ni_{0.25}Mn_{0.4}Ti_{0.15}O_2$	P2(40%), O3(60%)	142.9 mAh g^{-1}/0.1 C/2.0–4.5 V	85.6%/200cycles/1 C	[33]
P2/O3-$Na_{0.8}Ni_{0.23}Fe_{0.34}Mn_{0.43}O_2$	P2(10.1%), O3(89.9%)	146.4 mAh g^{-1}/0.1 C/2.0–4.0 V	93.1%/200cycles/1 C	[86]
P2/O3-$NaLi_{1/3}Mn_{2/3}O_2$	P2(27%), O3(73%)	226 mAh g^{-1}/0.05 C/1.5 V–4.5 V	84.37%/100cycles/1 C	[87]
P2/O3 – $Na_{0.8}Li_{0.03}Mg_{0.05}Ni_{0.28}Fe_{0.05}Mn_{0.54}Ti_{0.05}O_2$	P2(28.9%), O3(71.1%)	146 mAh g^{-1}/0.1 C/2.2–4.4 V	85.5%/100cycles/1 C	[88]
P2-$Na_{2/3}MnO_2$–coated O3-$NaNi_{0.5}Mn_{0.5}O_2$	P2(5%), O3(95%)	119.4 mAh g^{-1}/0.1 C/2.0–4.0 V	85.2%/1000cycles/5 C	[20]

hinder phase transitions, with the adjacent transition metal slabs in the P2 phase remaining stationary. This interaction generates stress opposite to the gliding direction at the phase boundary, preventing TMO_2 slab displacement in the P3 phase. As a result, even under significant sodium extraction, the material retains structural stability with minimal phase transformation.

As shown in Figure 2b, after multiple charge/discharge cycles, the P2 single-phase material experienced a significant volume change of 23.3%, whereas the P2 phase within the P2/O3 biphasic material exhibited a much lower volume change of only 8.7%. This can be attributed to the relatively low formation energy and stable structural evolution of the P2/O3 biphasic cathode, which collectively contribute to minimizing volumetric changes. Severe volume fluctuations are directly linked to crack formation and Mn dissolution, both of which degrade performance. Crack formation can be observed through SEM and TEM images, where SEM provides direct visualization of morphological changes, while TEM, combined with SAED patterns, offers detailed structural insights. As shown in Figure 2c, cracks develop in single-phase materials after prolonged cycling, whereas the P2/O3 biphasic cathode retains well-defined lattice fringes without crack formation. Manganese (Mn), a crucial element in cathode materials due to its ability to enhance structural stability, is consistently incorporated into the P2/O3 biphasic structure. Despite this, Mn-based P2 materials suffer from Mn dissolution during extended cycling, which negatively impacts cycle life. To overcome this issue, significant research has focused on suppressing Mn dissolution.[42, 43] The P2/O3 biphasic structure effectively mitigates this issue by maintaining phase stability over extended cycling, thereby minimizing structural deformation and volumetric changes. For instance, Li- and Ti-co-doped P2/O3 materials have demonstrated a high Mn/Fe molar ratio of 90.5%, indicating reduced Mn dissolution and improved structural integrity (Figure 2d).

Based on comparative analysis of in-situ XRD data, it has been observed that the phase stability and structural integrity of biphasic materials are further influenced by the applied voltage range. Specifically, setting the cut-off voltage to a relatively low value of 4 V or narrowing the voltage range promotes the formation of a P2/P3 phase at the end of the charge.[29, 38, 51] In contrast, applying a cut-off voltage above 4.2 V induces the formation of OP4/P3 or OP4/OP2 biphasic structures at the end of the charge.[28, 39, 40, 45] Importantly, all biphasic materials were found to revert to their original phases reversibly during the discharge process. Notably, even at a high voltage of 4.5 V, when the P2 phase constitutes approximately 90% within the P2/O3 structure, phase transitions P2/O3 - P2 - P2/O3 can occur without forming an intermediate OP4 (or Z) phase.[41]

Under the assumption that the original phase is reversibly recovered during the discharge process, it might seem intuitive to infer that more extensive phase changes would extract more sodium ions, thereby enhancing capacity. However, this inference is invalid. As shown in Figure 2e, at the end of the charging process, nearly at 4.5 V, $Na_{0.76}$ biphasic cell(37.8% P2) forms OP4/P3 structure, while $Na_{0.80}$ biphasic cell(14.3% P2) forms OP4/OP2 phase. By suppressing the P3–OP2 phase transition, the $Na_{0.76}$ biphasic cell demonstrates a higher capacity of 115 mAh g^{-1} compared to the 85 mAh g^{-1} exhibited by the $Na_{0.80}$ cell.[33] First-principles calculations comparing the formation energy of the phases in the deeply sodiated state show that $Na_{0.76}$ energetically prefers the P2/P3 phases, whereas $Na_{0.80}$ favors the OP4/OP2 phases, explaining the observed differences in phase transitions (Figure 2f). The P2 phase within the P2/O3 biphasic cathode plays a critical role in stabilizing the material structure and suppressing slab gliding in the P3 phase under deep desodiation. Thus, the P2/O3 ratio is a key factor in maintaining structural stability and enhancing capacity. Furthermore, rather than comparing within P2/O3 materials, DFT calculations reveal that the average formation energy of the P2/O3 biphasic structure is lower than that of its single-phase counterparts (P2 and O3), making the biphasic structure more thermodynamically favorable.[31] Conversely, the migration energy of oxygen in P2/O3 materials is significantly higher compared to single-phase analogs, resulting in restricted oxygen migration due to the complex structure. This restriction facilitates reversible anionic activity within the biphasic system.[31]

© 2025 The Authors. ChemElectroChem published by Wiley-VCH GmbH

In conclusion, the P2/O3 biphasic structure offers enhanced structural stability, reduced Mn dissolution, and reliable reversible phase transitions, thereby significantly improving electrochemical performance and cycle longevity compared to single-phase materials.

2.3. Kinetics

In sodium-ion batteries, Na^+ diffusion kinetics are critical as they directly influence the rate capability and overall performance of the battery. In contrast to P2-layered oxide materials, O3-type materials exhibit two distinct sodium-ion diffusion pathways depending on the location of Na vacancies: the dumbbell hop and the tetrahedral hop (Figure 3a). Although the dumbbell hop might intuitively seem to require lower activation energy (E_a) due to the direct migration of sodium ions into a vacancy, it is actually energetically unfavorable.[44] This is because the sodium ions encounter significant interference from oxygen interactions along the migration path, resulting in higher activation energy and slower kinetics compared to the tetrahedral hop.[82, 83] Using NEB calculations (Figure 3b), differences in diffusion pathways and formation energies between single-phase materials (P2 and O3) and co-doped P2/O3 biphasic materials were identified. The P2 phase within the co-doped P2/O3 biphasic cathode shows similar crystal parameters to the pristine $Na_{0.7}MnO_2$ P2 phase, resulting in a comparable energy barrier. However, for pristine O3-$NaMn_{0.5}Ni_{0.5}O_2$, doping causes an expansion of the c-lattice parameter and the Na interlayer, leading to a shift in the diffusion pathway towards the more energetically favorable tetrahedral hop. Consequently, when the P2 and O3 phases

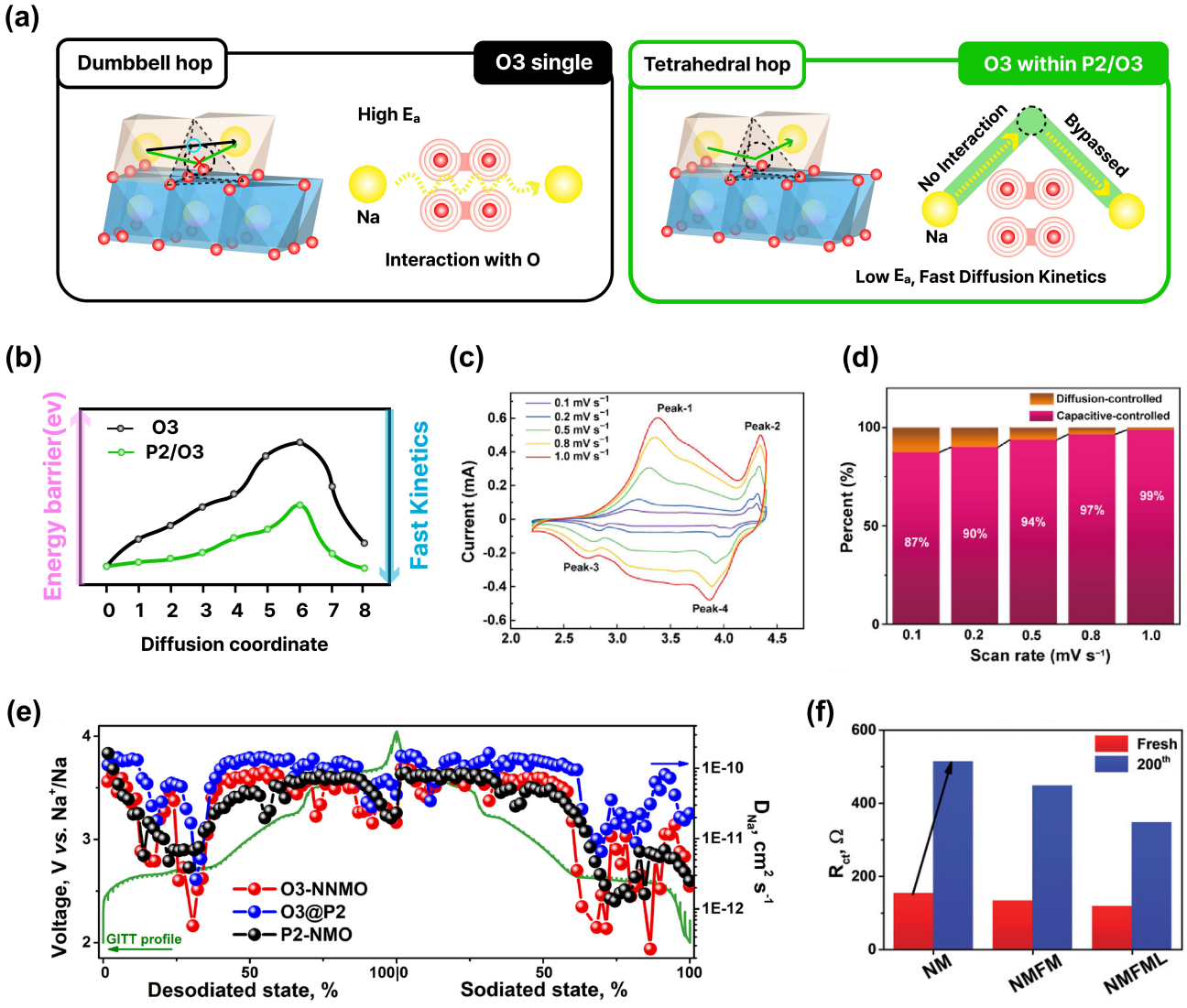


Figure 3. (a) Diffusion paths of O3-type material considering two mechanisms: dumbbell hop and tetrahedral hop. (b) Migration energy barriers for Na-ion diffusion using NEB calculations Reproduced with permission from ref [45]. Copyright 2023, Elsevier. (c) CV profiles of P2/O3-NMT_3 between 2.2 and 4.4 V at different scan rates. Reproduced with permission from ref [23]. Copyright 2022, Elsevier. (d) Ratio of the pseudo-capacitive and diffusion-controlled capacities of P2/O3-NMT_3 electrode at different scan rates. Reproduced with permission from ref [23]. Copyright 2022, Elsevier. (e) Voltage profile and calculated D_{Na^+} values based on GITT measurements. Reproduced with permission from ref [20]. Copyright 2022, Elsevier. (f) Charge transfer resistance of NM, NMFM, and NMFML cathodes before and after 200 cycles. Reproduced with permission from ref [46]. Copyright 2022, Wiley-VCH.

© 2025 The Authors. ChemElectroChem published by Wiley-VCH GmbH

21960216, 2025, 7, Downloaded from https://chemistry-europe.onlinelibrary.wiley.com/doi/10.1002/celc.202400657 by Ewha Womans University Library, Wiley Online Library on [10/08/2025]. See the Terms and Conditions (https://onlinelibrary.wiley.com/terms-and-conditions) on Wiley Online Library for rules of use; OA articles are governed by the applicable Creative Commons License

coexist, the O3 phase adopts the energetically preferred tetrahedral hopping pathway.

In addition to modeling and computational predictions of kinetics, various experimental techniques such as cyclic voltammetry (CV), galvanostatic intermittent titration technique (GITT), and electrochemical impedance spectroscopy (EIS) were employed to demonstrate the superior kinetics of the P2/O3 biphasic cathode. As shown in Figure 3c, CV at different scan rates was conducted to investigate the Na^+ diffusion kinetics. By fitting the oxidation peaks of the CV data and applying the Randles–Sevcik equation, $i = av^b$ (where i and v represent the current and scan rate), the diffusion- and capacitive-controlled capacities were calculated. The average value of the parameter b for P2/O3-NMT_3 was determined to be 0.8798, which is higher than the value for P2-NM (0.7455). Furthermore, as the scan rate increased, the capacitive contribution rose steadily, reaching up to 99% (Figure 3d). These results indicate that the P2/O3 material exhibits a higher capacitive contribution and superior Na^+ diffusion kinetics in the Na^+ storage mechanism compared to the P2-NM material.

GITT measurements were performed to evaluate the Na^+ diffusion coefficient (D_{Na^+}) at quasi-equilibrium potentials, providing insight into how the heterostructure influences cell performance. The average D_{Na^+} of the O3@5%P2 cathode ($1.13\times10^{-10}\,cm^2s^{-1}$) is approximately twice that of the O3-NNMO ($5.29\times10^{-11}\,cm^2s^{-1}$) and P2-NMO ($4.65\times10^{-11}\,cm^2s^{-1}$) cathodes, highlighting the superior reaction kinetics of the heterostructured material (Figure 3e). This enhanced Na^+ diffusion coefficient is attributed to the P2-NMO coating, which provides smooth Na-ion diffusion pathways. Furthermore, even conventional biphasic cathodes without a specific heterostructure exhibit smoother voltage profiles, lower polarization, and higher diffusion coefficients compared to single-phase cathodes.[47–49]

Charge transfer resistance (R_{ct}) obtained through EIS is associated with the efficiency of electron and ion transfer between the cathode and electrolyte.[50] A lower R_{ct} signifies improved electrochemical performance and faster charge/discharge kinetics, making it a crucial parameter for evaluating the diffusion kinetics of P2/O3 materials. As shown in Figure 3f, the P2/O3-NMFML exhibits a lower R_{ct} compared to the P2-NM in its pristine state, and this discrepancy becomes more pronounced after 200 cycles. This improvement can be attributed to the co-doping of Fe, Li, and Mg in the NM material, which facilitates the formation of a robust cathode-electrolyte interphase (CEI), resulting in enhanced electrochemical kinetics and faster Na^+ conductivity. The improved ionic dynamics of NMFML can be credited to its smooth phase transitions and stable crystal structure, where multi-element co-dopants suppress long-range cation ordering and maintain electrostatic equilibrium during deep desodiation.

2.4. Electrochemical Analysis

In the previous section, we discussed the superior diffusion kinetics and thermodynamic stability exhibited by the P2/O3 biphasic cathode compared to single-phase materials such as P2 and O3. Electrochemical tests on P2/O3 biphasic half-cells provide a comprehensive evaluation of their enhanced performance, including key metrics such as capacity, rate capability, and long-term cycling stability. This section aims to provide a comparative analysis of the electrochemical performance of P2/O3 biphasic cells against single-phase cells, leveraging the thermodynamic and kinetic characteristics previously discussed.

Table 1 highlights that, unlike Ni, Mn-based layered oxide cathodes with a single P2 or O3 phase, P2/O3 biphasic cathodes exhibit superior battery performance, characterized by higher reversible capacity and excellent capacity retention even at high C-rates.[3, 23, 36] Particularly when operating at voltages exceeding 4.2 V, O3-based cathodes display high initial capacity but suffer from significant fading, while P2-based cathodes exhibit better retention but lower initial capacity. In contrast, P2/O3 biphasic cathodes effectively combine the advantages of both phases, delivering stable capacity and exceptional rate capability under high-voltage conditions.

The phase transition behavior in P2/O3 biphasic materials is critically dependent on the ratio of the P2 phase, as mentioned earlier. For example, the P2/O3 biphasic cathode cell with an optimized P2/O3 ratio ($Na_{0.76}$) exhibits thermodynamically stable phase transitions, leading to superior long-term cycling stability, especially at elevated voltages. In contrast, a P2/O3 biphasic cathode cell with suboptimal ratio, such as $Na_{0.80}$, demonstrates notably lower capacity retention at high voltages (around 4.5 V) compared to the single-phase O3 ($Na_{0.84}$) and P2 ($Na_{0.62}$) cells (Figure 4a). This highlights the pivotal role that sodium content and phase ratio play in determining the electrochemical performance and stability of P2/O3 biphasic materials. Moreover, both the sodium content and choice of dopants significantly influence the cyclability of the cell. As shown in Figure 4b, an NMFML Na half-cell demonstrates the highest reversible capacity and excellent capacity retention (87.3% after 100 cycles at 1 C).

The introduction of electroactive Fe reduces the Mn content, while electrochemically inactive Mg disrupts in-plane ordering, thereby enhancing structural stability.[52, 54] Furthermore, low-valent Li contributes to structural stability by facilitating Mn oxidation through charge compensation, which also increases Na content, thereby improving reversible capacity.[53] This co-doping strategy demonstrates a synergistic effect, yielding better structural integrity and enhanced electrochemical performance compared to single-element doping. Rate capability tests also show that the performance of the P2/O3 biphasic cell surpasses that of single-phase cells (Figure 4c). Notably, $Na_{7/9}Ni_{2/9}Mn_{4/9}Fe_{1/9}Mg_{1/9}Li_{1/9}O_2$ (NMFML) outperforms $Na_{2/3}Ni_{2/9}Mn_{5/9}Fe_{1/9}Mg_{1/9}O_2$ (NMFM), primarily due to the strong Li–O bonding, which prevents structural collapse, and promotes the formation of a robust cathode-electrolyte interphase that reduces impedance and improves diffusion kinetics.

Doping with high-valent transition metals further enhances the performance of P2/O3 biphasic cathodes compared to single-phase cells. As seen in Figure 4d, the GCD profile of the P2/O3 biphasic cell differs markedly from that of single-phase cells. The P2-NaNM electrode exhibits distinct plateaus associ-

© 2025 The Authors. ChemElectroChem published by Wiley-VCH GmbH

21960216, 2025, 7, Downloaded from https://chemistry-europe.onlinelibrary.wiley.com/doi/10.1002/celc.202400657 by Ewha Womans University Library, Wiley Online Library on [10/08/2025]. See the Terms and Conditions (https://onlinelibrary.wiley.com/terms-and-conditions) on Wiley Online Library for rules of use; OA articles are governed by the applicable Creative Commons License

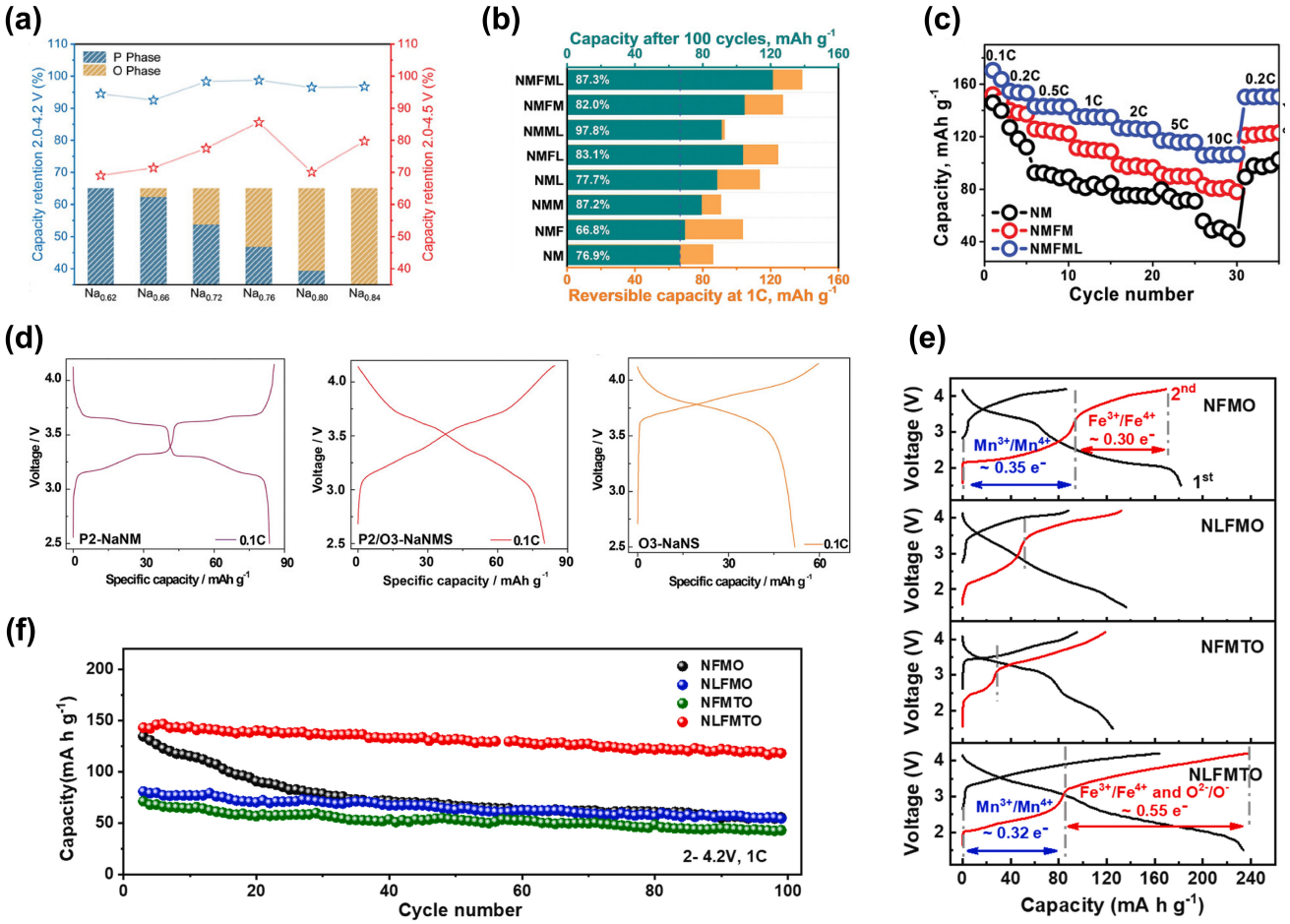


Figure 4. (a) Capacity retention rate of $Na_xCu_{0.1}Co_{0.1}Ni_{0.25}Mn_{0.4}Ti_{0.15}O_2$ cathodes with different sodium content under different voltage ranges. Reproduced with permission from ref [33]. Copyright 2024, Wiley-VCH. (b) Cycling stability of half cells featuring different multicomponent cathodes. Reproduced with permission from ref [46]. Copyright 2022, Wiley-VCH. (c) Rate capability at different current rates from 0.1 to 10 C. Reproduced with permission from ref [46]. Copyright 2022, Wiley-VCH. (d) Galvanostatic charge/discharge (GCD) curves vs. specific capacity of P2/O3-NaNMS compared with P2-NaNM, O3-NaNS at 0.1 C. Reproduced with permission from ref [51]. Copyright 2022, Wiley-VCH. (e) The 1st and 2nd charge-discharge curves at 0.1 C within the voltage range of 1.5–4.2 V, and (f) the cycling performance at 1 C within the voltage range of 2.0–4.2 V for NFMO, NLFMO, NFMTO, and NLFMTO. Reproduced with permission from ref [34]. Copyright 2021, Elsevier.

ated with Na^+/vacancy ordering and phase transitions, while the P2/O3-NaNMS electrode displays smoother curves, indicating a solid-solution reaction without severe phase transitions during the charge/discharge process. Furthermore, the O3-NaNS material, due to its high midpoint voltage, exhibits lower specific capacity and energy density compared to the P2/O3-NaNMS. This behavior is attributed to Sn's role in suppressing the gliding of transition metal layers and effectively modulating the hybridization between the orbitals of oxygen and transition metal atoms.

Even within the same voltage range, the presence of anion redox activity varies depending on the dopant used. For example, during charge/discharge cycles between 1.5 V and 4.2 V, only the P2/O3-NLFMTO electrode utilizes O^{2-}/O^- redox couples at higher potentials, resulting in increased capacity (Figure 4e). Additionally, its cycling stability over 100 cycles significantly surpasses that of other cells (Figure 4f). This superior performance is attributed to the substitution of Mn with Ti, which forms strong Mn–O–Ti–O–Fe bonds that suppress Jahn-Teller distortion and mitigate structural degradation.

In conclusion, P2/O3 biphasic cathodes successfully integrate the complementary advantages of P2 and O3 phases, offering a balance between structural stability, capacity retention, and rate capability under a wide range of operating conditions.

3. Other Biphasic Cathodes

Recent research has increasingly concentrated on the P2/O3 biphasic cathode, which has attracted considerable interest. However, several biphasic cathode systems, including P2/P3, P3/O3, P2/P′2, and P2/O′3, are also actively being investigated. Additionally, studies have explored biphasic cathodes that combine layered oxides (P2 and O3) with other structures like tunnel or spinel. For instance, Zhuang-chun et al. developed a high energy density layered-tunnel $Na_{2/3}Mn_{8/9}Ti_{1/9}O_2$ material

© 2025 The Authors. ChemElectroChem published by Wiley-VCH GmbH

21960216, 2025, 7, Downloaded from https://chemistry-europe.onlinelibrary.wiley.com/doi/10.1002/celc.202400657 by Ewha Womans University Library, Wiley Online Library on [10/08/2025]. See the Terms and Conditions (https://onlinelibrary.wiley.com/terms-and-conditions) on Wiley Online Library for rules of use; OA articles are governed by the applicable Creative Commons License

utilizing a dual-function strategy, which exhibited notable moisture stability and enhanced cycling performance.[55] Similarly, Sai et al. reported a Mn-rich layered-spinel composite stabilized through Mo doping, effectively alleviating the P2-P2″ phase transition at higher voltages.[56] While this review primarily focuses on the P2/O3 system, we also present a brief overview of other biphasic cathodes. In the following section, we discuss how these systems differ from the well-studied P2/O3 cathode.

3.1. P2/P3 Biphasic Cathode

The P3 structure differs from the P2 phase by exhibiting an ABCABC stacking sequence (Figure 5a). Thermodynamically, the P3 structure stabilizes at sintering temperatures below 800 °C, while the P2 phase becomes favorable at temperatures above this threshold.[60] P3-type cathodes generally demonstrate superior rate performance compared to the P2 structure, despite possessing lower crystal symmetry.[58, 61, 62] This advantage stems from the P3 structure's relatively wider interlayer spacing and more flexible ion diffusion pathways, leading to a higher diffusion coefficient.[63] However, the P3 materials also undergo irreversible P3–P″3 phase transitions during the cycle. Various strategies have been investigated to address this issue, including the introduction of vacancies in the transition metal (TM) layer.[64] One promising approach involves forming P2/P3 or P3/O3 biphasic cathodes through ion substitution. Zichao et al. developed a hydrostable Zn-doped P2@P3 biphasic structure using a simple sol-gel method, which demonstrated

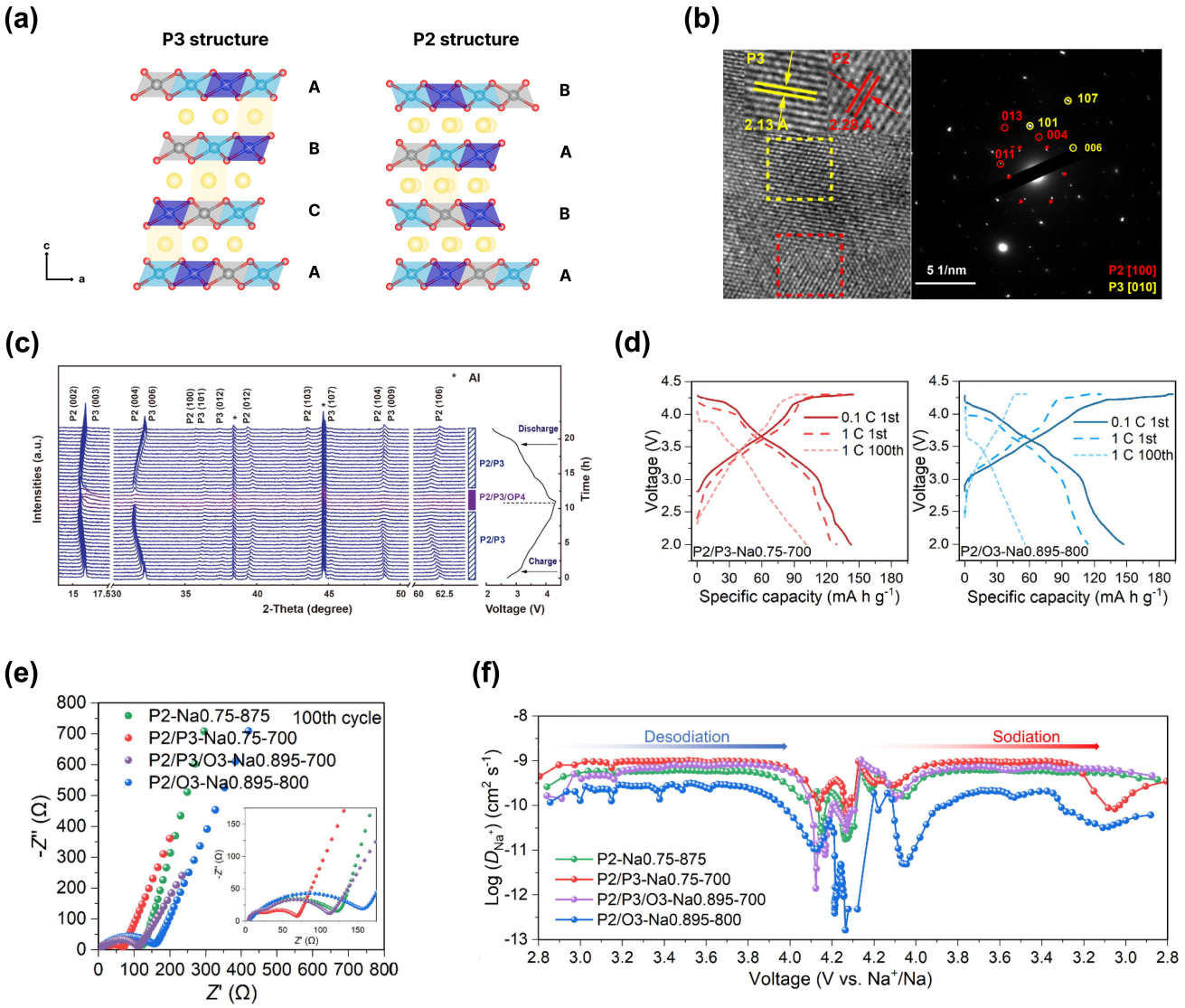


Figure 5. (a) Layered structures of P2 (left) and P3 (right). Reproduced with permission from ref [57]. Copyright 2018, American Chemical Society. (b) HRTEM images, as well as SAED pattern of P2/P3-NLNMM and superstructure reflections are indicated by red stars. Reproduced with permission from ref [58]. Copyright 2018, Elsevier. (c) In-situ XRD patterns collected during the 1st cycle of P2/P3-NLMNM cathode under a 0.1 C-rate. Reproduced with permission from ref [58]. Copyright 2018, Elsevier. (d) Charging/discharging of P2/P3- and P2/O3- biphasic cathodes. Reproduced with permission from ref [59]. Copyright 2024, Elsevier and Science Press. (e) EIS and (f) GITT curves of P2-, P2/P3-, P2/O3-, and P2/P3/O3 cathode materials. Reproduced with permission from ref [59]. Copyright 2024, Elsevier and Science Press.

© 2025 The Authors. ChemElectroChem published by Wiley-VCH GmbH

21960216, 2025, 7, Downloaded from https://chemistry-europe.onlinelibrary.wiley.com/doi/10.1002/celc.202400657 by Ewha Womans University Library, Wiley Online Library on [10/08/2025]. See the Terms and Conditions (https://onlinelibrary.wiley.com/terms-and-conditions) on Wiley Online Library for rules of use; OA articles are governed by the applicable Creative Commons License

improved structural stability and humidity resistance.[65] In Section 3.1, we discuss P2/P3 biphasic cathodes, followed by an analysis of P3/O3 biphasic cathodes in Section 3.2.

Figure 5b illustrates high-resolution transmission electron microscopy (HRTEM) data, revealing interplanar spacings of 2.13 Å for the P3 phase and 2.28 Å for the P2 phase, corresponding to the P3(104) and P2(012) crystal planes with distinct lattice fringes. Additionally, the selected area electron diffraction (SAED) pattern confirms the polycrystalline nature of the sample, consistent with the HRTEM observations. Bright diffraction spots along the [010] direction correspond to characteristic reflections of the P3 layered structure, while those along the [100] direction are attributed to the diffraction pattern of the P2 phase.

As indicated by the in-situ XRD data in Figure 5c, the P2/P3 structure maintains stability up to a charging voltage of 4.2 V. Beyond this point (4.21 V), the P2 phase transforms into the OP4 phase. Similar to the behavior observed in P2/O3 biphasic cathode, the formation of the OP4 intermediate phase alleviates structural stress through sliding layers, facilitated by the stabilizing effects of Li and Mg, compared to the direct P2/P3 to O2/P′3 phase transition. The highly reversible nature of this phase transformation significantly enhances structural stability during prolonged cycling.

In some cases, P2/P3 materials exhibit better performance than P2/O3 biphasic materials. For example, Feifei et al. developed a synthetic hybrid P2/P3-$Na_{0.75}Ni_{0.25}Mn_{0.75}O_2$ material, which combines the benefits of both P2 and P3 structures while overcoming their respective limitations, resulting in remarkable electrochemical performance.[59] As shown in Figure 5d, the initial specific discharge capacities of P2/P3-$Na_{0.75}$-700 and $Na_{0.895}$-800 were 142.6 and 147.0 mAh g^{-1}, with initial Coulombic efficiencies of 98.72% and 76.28%, respectively. Although P2/O3-$Na_{0.895}$-800 exhibits a higher initial specific discharge capacity, it suffers from rapid capacity decay due to the limited presence of the O3 phase on its surface. While the O3 phase contributes to the material's capacity, it also induces detrimental phase transitions that accelerate capacity degradation.

From a kinetic perspective, EIS and GITT analyses show that the P2/P3 biphasic cathode outperforms the other multiphase materials including P2/O3 biphasic cathode in both diffusion coefficient and impedance. P2/P3-$Na_{0.75}$-700 consistently exhibits the lowest R_{CEI} and R_{ct}, reflecting its superior Na^+ transfer rate and high efficiency in sustaining rapid Na^+ transport throughout extended cycling.[59] After 100 cycles, the charge transfer impedance of P2/O3-$Na_{0.895}$-800 shows a notable increase (Figure 5e). Additionally, Figure 5f highlights that the average Na^+ diffusion coefficient of P2/P3-$Na_{0.75}$-700 (5.89×10^{-10} $cm^2 s^{-1}$) is much higher than that of P2/O3-$Na_{0.895}$-800 (1.13×10^{-10} $cm^2 s^{-1}$). This clearly shows that the Na^+ transport kinetics of P2/O3-$Na_{0.895}$-800 are inferior, particularly in the high-voltage region where irreversible phase transitions occur and the reduced layer spacing hinders Na^+ diffusion. Therefore, as mentioned in Section 2.4, synthesizing biphasic cathodes, including P2/O3 systems, with an appropriate phase ratio is crucial to optimizing performance.

3.2. P3/O3 Biphasic Cathode

P3/O3 riveting structure effectively mitigates the rigid failure caused by phase transition. Meanwhile, O3/P3 phases provide the main storage sites for Na^+ as skeletons and the existence of P3 phase provides a better diffusion pathway for ion transport.[66] Additionally, the P3 phase structurally resembles the O3 phase, allowing the O3 phase to easily transform into the P3 phase through a simple sliding of the TMO_2 layer, and vice versa.[68–71] It means that P3/O3 biphasic cathodes undergo reversible phase transition during cycling. The P3/O3 structure can be formed through doping with various elements.

As depicted in the schematic diagram of the molybdenum-doped crystal structure in the combined mode (Figure 6a), a gradual transition from the O3 phase to the P3 phase is observed while maintaining a well-defined crystal structure between the two phases. TEM image clearly shows the regions corresponding to the P3 phase, O3 phase, and the boundary between these two phases (Figure 6b). Measurements of the crystal plane spacing corresponding to the (003) lattice plane indicate values of 5.57 nm, 5.43 nm, and 5.52 nm for the P3, O3, and boundary regions, respectively. This suggests that while the boundary exhibits a complex crystal structure, it tends to resemble the P3 phase structurally. However, the stability of the P3/O3 structure is contingent on thermodynamic favorability. For instance, Aniruddh et al. reported that Ni-doped P3/O3 NFNM cathodes demonstrated superior sodium storage performance by maintaining a stable P3 phase at high voltages, attributed to enhanced hole conductivity, thereby outperforming the P3/O3 NFM material.[72] The structural evolution of the stable P3/O3 biphasic half-cell can be monitored by the in-situ XRD data presented in Figure 6c.

At lower voltages (<4.0 V), P3/O3 structure undergoes an O3-P3 phase transition as with other O3 phase materials. However, at higher voltages (4.0–4.25 V), simultaneous O3-P3 and P3-Hex.O3′ phase transitions occur, with smaller volumetric changes during Na^+ deintercalation compared to pure O3 materials. Even after the first cycle, the P3/O3 structure exhibits reversible phase transitions without severe degradation. This stable phase transition behavior is closely related to the formation energy of each phase. DFT calculation confirms that the total DFT calculation confirms that the total energy of O3-type $Na_{2/3}Ni_{1/3}Mn_{2/3-x}Ti_xO_2$ changes as the Ti content increases (Figure 6d). Notably only at $x=1/3$ does the O3 phase exhibit thermodynamic energy comparable to that of the P3 counterpart, which explains the possibility to form the stable P3/O3 structure. Additionally, over 1000 cycles, the P3/O3 biphasic material($x=1/3$) demonstrates superior capacity retention of 78%, outperforming the single-phase P3 material with lower Ti content (Figure 6e).

Beyond Ti or Mo single-element doping, superior low-temperature performance can also be achieved in P3/O3 structures through LiF incorporation. Heramba et al. demonstrated that even at subzero temperatures (−20 °C), capacity retention reached 94% of the initial value. This performance was attributed to enhanced structural stability, reduced Jahn-

© 2025 The Authors. ChemElectroChem published by Wiley-VCH GmbH

21960216, 2025, 7, Downloaded from https://chemistry-europe.onlinelibrary.wiley.com/doi/10.1002/celc.202400657 by Ewha Womans University Library, Wiley Online Library on [10/08/2025]. See the Terms and Conditions (https://onlinelibrary.wiley.com/terms-and-conditions) on Wiley Online Library for rules of use; OA articles are governed by the applicable Creative Commons License

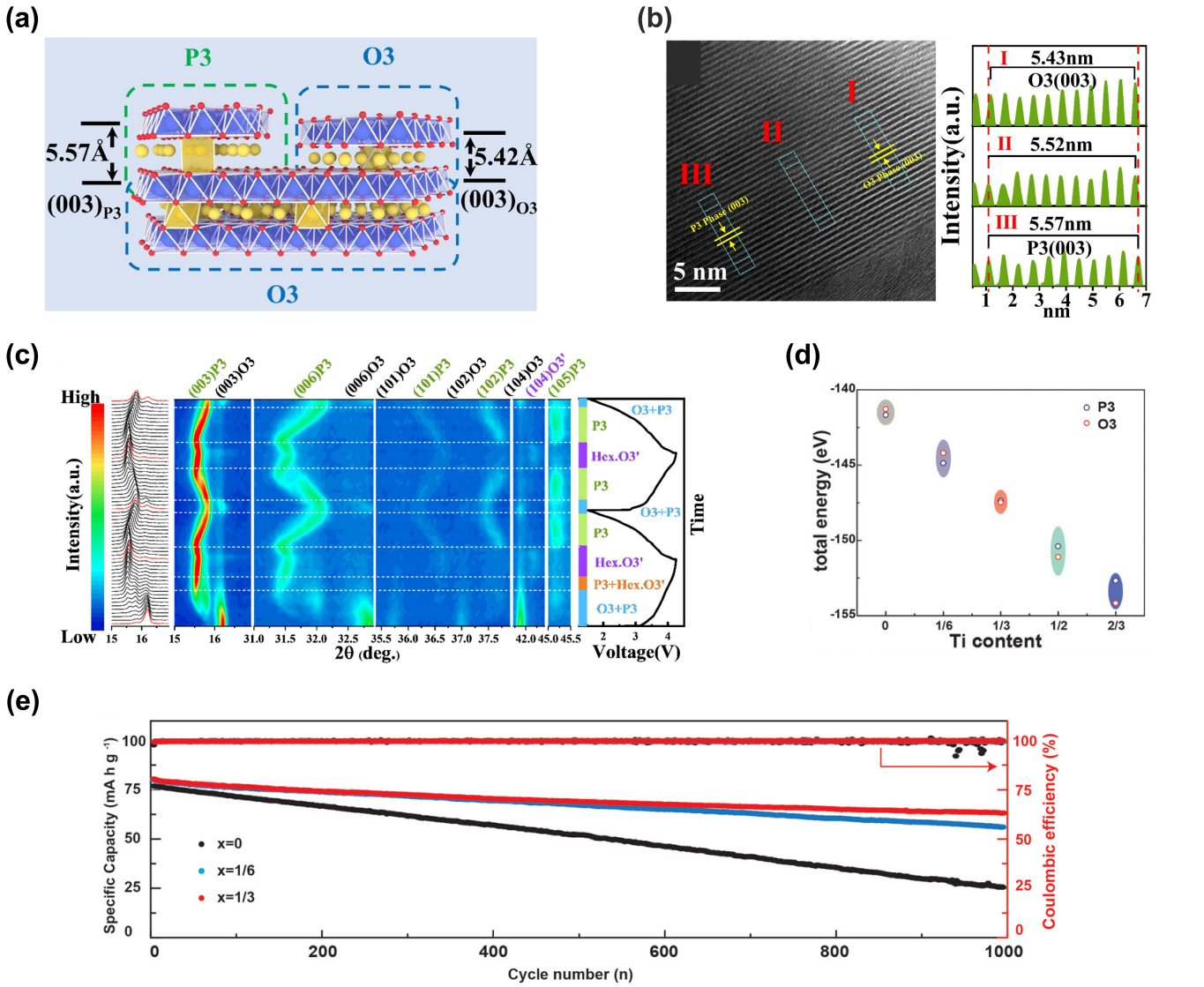


Figure 6. (a) Schematic diagram of O3 and P3 phase structures, (b) HRTEM image of O3/P3 biphasic structures and corresponding line profile, (c) Structure evolutions by 2D maps and potential profiles of in-situ XRD spectra collected during the 1st and 2nd charge–discharge in the voltage range of 1.5–4.25 V of P3/O3 biphasic cathode. Reproduced with permission from ref [66]. Copyright 2024, Elsevier. (d) The calculated total energies of a series of Ti-substituted P3/O3 cathodes with different Ti content. (e) Specific capacity with Coulombic efficiency of three cathodes during 1000 cycles at 1 C. Reproduced with permission from ref [67]. Copyright 2021, Wiley-VCH.

Teller distortions, and improved Na^+ kinetics, facilitating Na^+ transport across a wide range of temperatures.[73]

3.3. Biphasic Cathode with Distorted Phase: P′2 or O′3

Biphasic cathode systems incorporating distorted phases such as P′2 and O′3 have demonstrated significant performance enhancements, particularly when coexisting with conventional structures like P2 or O3. These distorted phases, derived from $NaMnO_2$ (NMO) materials under specific conditions, exhibit monoclinic symmetries – C2/c for P′2 and C2/m for O′3 (Figure 7a) – in contrast to the hexagonal symmetries of their parent phases, P2 [$P6_3/mmc$] and O3 [R3m]. This structural distortion, primarily resulting from slab sliding within the crystal lattice, introduces unique electrochemical behaviors that are advantageous for sodium-ion batteries.

The P′2 and O′3 phases share structural similarities with P2 and O3, respectively, but differ significantly in their sodium ion coordination environments. In the P′2 phase, sodium ions are off-centered within trigonal prisms, altering the Mn–Na distances and impacting electrostatic interactions.[75] Conversely, in the P2 phase, sodium ions are centrally aligned within the prisms, resulting in different dynamics. These distinctions influence electrochemical performance and cycling stability, making the P′2 phase particularly valuable for enhancing material performance in biphasic configurations.

The synergistic effects observed in biphasic cathodes such as P2/O′3 systems highlight the complementary roles of each phase. The P2 phase offers rapid ion kinetics, while the O′3

© 2025 The Authors. ChemElectroChem published by Wiley-VCH GmbH

21960216, 2025, 7, Downloaded from https://chemistry-europe.onlinelibrary.wiley.com/doi/10.1002/celc.202400657 by Ewha Womans University Library, Wiley Online Library on [10/08/2025]. See the Terms and Conditions (https://onlinelibrary.wiley.com/terms-and-conditions) on Wiley Online Library for rules of use; OA articles are governed by the applicable Creative Commons License

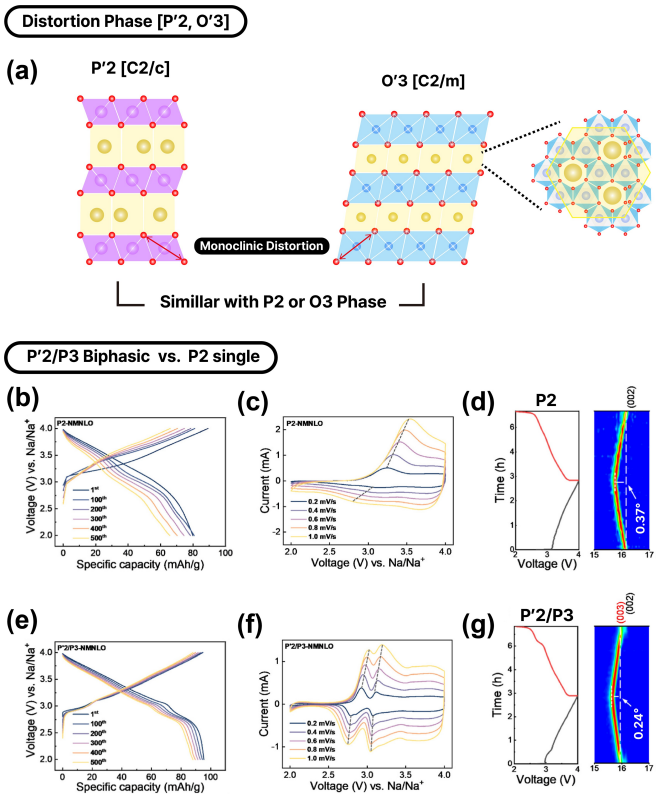


Figure 7. (a) Schematic illustration of the P′2, O′3 layered structure. (b) Charge and discharge curve, (c) CV curves at different scan rate, (d) In-situ XRD characterization of P2-NMNLO. Reproduced with permission from ref [81]. Copyright 2024, American Chemical Society. (e) Charge and discharge curve, (f) CV curves at different scan rate, (g) In-situ XRD characterization of P′2/P3-NMNLO. Reproduced with permission from ref [81]. Copyright 2024, American Chemical Society.

phase provides higher capacity, resulting in improved overall performance.[76–78] Strategies to optimize these systems include adjusting sodium content to tailor the P2/O′3 phase ratio and doping with transition metals like Cu and Zn, enhancing electrochemical properties.[74,79] In these systems, sodium ions reside in trigonal prismatic sites within the P2 structure and octahedral sites in the O′3 structure, facilitating efficient diffusion pathways and contributing to enhanced capacity and reversibility. Notably, biphasic P2/O′3 cathodes exhibit superior long-term cycling performance compared to single-phase materials. For instance, the P2/O′3 $Na_{0.6}[Mn_{0.5}Co_{0.25}Sb_{0.25}]O2$ (NMCSO) cathode retains a high capacity of 98 mAh g^{-1} even after extended cycling at high rates, significantly outperforming single-phase counterparts.[74] Structural analysis reveals that the P2 phase buffers volume fluctuations within the O′3 phase, thereby enhancing its structural stability and reducing lattice parameter changes during charge–discharge cycles.

The P′2/P3 system similarly demonstrates notable advantages in terms of electrochemical performance and structural robustness. Compared to single-phase P2 materials (Figure 7b), the P′2/P3 configuration exhibits higher initial capacity and superior capacity retention over extended cycles. For example, the P′2/P3-NMNLO electrode retains 88.1 mAh g^{-1} after 500 cycles with a retention rate of 92.3 %, significantly surpassing the performance of single-phase P2-NMNLO (Figure 7e). Cyclic voltammetry tests indicate reduced polarization and enhanced reversibility in P′2/P3-NMNLO (Figure 7c), as evidenced by smaller potential shifts and more stable oxidation/reduction peaks compared to P2-NMNLO (Figure 7f). This behavior reflects more complete utilization of Ni redox activity and improved sodium-ion mobility within the biphasic structure. In-situ XRD analyses of P′2/P3-NMNLO reveal a reversible phase transition sequence with minimal volume change compared with P2-NMNLO (Figure 7d), highlighting its structural stability and resistance to microcrack formation (Figure 7g). This stability mitigates mechanical strain at the P′2/P3 interface, contributing to enhanced cycling and rate capabilities. Additionally, the P3 phase compensates for sodium deficiencies in the P′2 structure, further enhancing overall performance.

These findings underscore the potential of biphasic cathodes incorporating distorted phases like P′2 and O′3 to achieve high capacity, structural robustness, and superior electrochemical dynamics, offering promising avenues for the development of advanced sodium-ion battery cathodes.

4. Summary and Outlook

Numerous studies have demonstrated that P2/O3 biphasic cathodes offer superior performance in both kinetic and thermodynamic aspects compared to single-phase materials. This enhanced performance arises from the synergistic combination of the fast ionic diffusion properties of the P2 phase and the high capacity of the O3 phase. However, synthesizing biphasic materials with better performance than single-phase counterparts is challenging, as it requires optimizing factors such as Na and TM content, synthesis methods, and sintering conditions. Specifically, the synthesis process plays a critical role in forming unique P2/O3 structures. To achieve the desired phase formation, Na and TM compositions must be carefully adjusted, and phase behavior can be predicted using concepts like cationic and radial potentials. Additionally, fine-tuning sintering parameters, including temperature, cooling rate, and atmosphere, is essential for optimizing phase stability and electrochemical performance. For example, appropriate quenching time (cooling rate) and precise atmospheric control have been shown to improve electrochemical performance by promoting a balanced P2/O3 ratio.

If the P2/O3 ratio is not appropriately balanced, the performance may degrade compared to single-phase materials. Mengting et al. proposed a structural evolution strategy involving Li^+ substitution, transitioning from biphasic to monophase $Na_{0.766+x}Li_xNi_{0.33-x}Mn_{0.5}Fe_{0.1}Ti_{0.07}O_2$ to enhance battery performance.[80] Nevertheless, if the P2 and O3 phases can be synthesized in an optimal ratio, and challenges such as complex electrochemical phase transitions and high-rate performance are effectively addressed, biphasic cathodes hold significant potential to outperform single-phase materials.

Beyond the P2/O3 system, other biphasic cathodes in sodium-ion batteries, such as P2/P3, P3/O3, and P2/O′3 structures, have also shown promising performance. However,

© 2025 The Authors. ChemElectroChem published by Wiley-VCH GmbH

21960216, 2025, 7, Downloaded from https://chemistry-europe.onlinelibrary.wiley.com/doi/10.1002/celc.202400657 by Ewha Womans University Library, Wiley Online Library on [10/08/2025]. See the Terms and Conditions (https://onlinelibrary.wiley.com/terms-and-conditions) on Wiley Online Library for rules of use; OA articles are governed by the applicable Creative Commons License

these systems remain less extensively investigated due to the stringent synthesis conditions they require. Future research should focus on exploring these alternative biphasic structures, as well as the development of multiphase cathode materials, including ternary-phase systems. Such advancements could unlock new pathways to further enhance battery performance, addressing key challenges such as capacity retention, structural stability, and rate capability. Ultimately, the continued exploration of biphasic and multiphase cathode materials holds significant promise for the advancement of next-generation sodium-ion batteries.

Acknowledgements

This work was supported by the National Research Foundation of Korea (NRF) grant funded by the Korea government (MSIT) (RS-2024-00404414), the National Research Foundation of Korea (NRF) grant funded by the Korea government (MSIT) (RS-2024-00422387) and the INNOPOLIS Foundation grant funded by the Korean government (MSIT) (INNOPOLIS2023-SB-SB-0011-02).

Conflict of Interests

The authors declare no conflict of interest.

Data Availability Statement

The data that support the findings of this study are available from the corresponding author upon reasonable request.

Keywords: sodium-ion batteries · biphasic cathodes · P2/O3 composites · layered oxides

[1] B. Dunn, H. Kamath, J.-M. Tarascon, *Science* **2011**, *334*, 928–935.
[2] Y. Kim, K.-H. Ha, S. M. Oh, K. T. Lee, *Chem. Eur. J.* **2014**, *20*, 11980–11992.
[3] J.-Y. Hwang, S.-T. Myung, Y.-K. Sun, *Chem. Soc. Rev.* **2017**, *46*, 3529–3614.
[4] W. Zuo, A. Innocenti, M. Zarrabeitia, D. Bresser, Y. Yang, S. Passerini, *Acc. Chem. Res.* **2023**, *56*, 284–296.
[5] Y. Xiao, P.-F. Wang, Y.-X. Yin, Y.-F. Zhu, X. Yang, X.-D. Zhang, Y. Wang, X.-D. Guo, B.-H. Zhong, Y.-G. Guo, *Adv. Energy Mater.* **2018**, *8*, 1800492.
[6] H. Ma, H. Su, K. Amine, X. Liu, S. Jaffer, T. Shang, L. Gu, H. Yu, *Nano Energy* **2018**, *43*, 1–10.
[7] Z. Liu, C. Zhou, J. Liu, L. Yang, J. Liu, M. Zhu, *Chem. Eng. J.* **2022**, *431*, 134273.
[8] H. Yang, D. Wang, Y. Liu, Y. Liu, B. Zhong, Y. Song, Q. Kong, Z. Wu, X. Guo, *Energy Environ. Sci.* **2024**, *17*, 1756–1780.
[9] C. Fouassier, C. Delmas, P. Hagenmuller, *Mater. Res. Bull.* **1975**, *10*, 443–449.
[10] K. Liu, S. Tan, J. Moon, C. J. Jafta, C. Li, T. Kobayashi, H. Lyu, C. A. Bridges, S. Men, W. Guo, Y. Sun, J. Zhang, M. P. Paranthaman, X.-G. Sun, S. Dai, *Adv. Energy Mater.* **2020**, *10*, 2000135.
[11] A. Konarov, H. J. Kim, J.-H. Jo, N. Voronina, Y. Lee, Z. Bakenov, J. Kim, S.-T. Myung, *Adv. Energy Mater.* **2020**, *10*, 2001111.
[12] F. Ding, C. Zhao, D. Zhou, Q. Meng, D. Xiao, Q. Zhang, Y. Niu, Y. Li, X. Rong, Y. Lu, L. Chen, Y.-S. Hu, *Energy Storage Mater.* **2020**, *30*, 420–430.
[13] Y. You, S. Xin, H. Y. Asl, W. Li, P.-F. Wang, Y.-G. Guo, A. Manthiram, *Chem.* **2018**, *4*, 2124–2139.
[14] E. Talaie, V. Duffort, H. L. Smith, B. Fultz, L. F. Nazar, *Energy Environ. Sci.* **2015**, *8*, 2512–2523.
[15] H. Ji, J. Zhai, G. Chen, X. Qiu, H. Fang, T. Zhang, Z. Huang, W. Zhao, Z. Wang, M. Chu, R. Wang, C. Wang, R. Li, W. Zeng, X. Wang, Y. Xiao, *Adv. Funct. Mater.* **2022**, *32*, 2109319.
[16] Y.-F. Zhu, Y. Xiao, W.-B. Hua, S. Indris, S.-X. Dou, Y.-G. Guo, S.-L. Chou, *Angew. Chem. Int. Ed.* **2020**, *59*, 9299–9304.
[17] G. Gao, D. Tie, H. Ma, H. Yu, S. Shi, B. Wang, S. Xu, L. Wang, Y. Zhao, *J. Mater. Chem. A* **2018**, *6*, 6675–6684.
[18] C. Chen, W. Huang, Y. Li, M. Zhang, K. Nie, J. Wang, W. Zhao, R. Qi, C. Zuo, Z. Li, H. Yi, F. Pan, *Nano Energy* **2021**, *90*, 106504.
[19] Y. Xiao, N. M. Abbasi, Y.-F. Zhu, S. Li, S.-J. Tan, W. Ling, L. Peng, T. Yang, L. Wang, X.-D. Guo, Y.-X. Yin, H. Zhang, Y.-G. Guo, *Adv. Funct. Mater.* **2020**, *30*, 2001334.
[20] X. Liang, T.-Y. Yu, H.-H. Ryu, Y.-K. Sun, *Energy Storage Mater.* **2022**, *47*, 515–525.
[21] C. Zhao, Q. Wang, Z. Yao, J. Wang, B. Sánchez-Lengeling, F. Ding, X. Qi, Y. Lu, X. Bai, B. Li, H. Li, A. Aspuru-Guzik, X. Huang, C. Delmas, M. Wagemaker, L. Chen, Y.-S. Hu, *Science* **2020**, *370*, 708–711.
[22] P. A. Maughan, A. B. Naden, J. T. S. Irvine, A. R. Armstrong, *Commun. Mater.* **2023**, *4*, 1–7.
[23] L. Yu, Z. Cheng, K. Xu, Y.-X. Chang, Y.-H. Feng, D. Si, M. Liu, P.-F. Wang, S. Xu, *Energy Storage Mater.* **2022**, *50*, 730–739.
[24] X. Gao, H. Liu, H. Chen, Y. Mei, B. Wang, L. Fang, M. Chen, J. Chen, J. Gao, L. Ni, L. Yang, Y. Tian, W. Deng, R. Momen, W. Wei, L. Chen, G. Zou, H. Hou, Y.-M. Kang, X. Ji, *Sci. Bull.* **2022**, *67*, 1589–1602.
[25] C. Zheng, D. Zhang, D. Zhang, J. Li, *Chem. Eng. J.* **2024**, *491*, 151858.
[26] C. Jiang, Y. Wang, Y. Xin, Q. Zhou, Y. Pang, B. Chen, Z. Wang, H. Gao, *J. Mater. Chem. A* **2024**, *12*, 13915–13924.
[27] R. Mishra, R. K. Tiwari, A. Patel, A. Tiwari, R. K. Singh, *J. Energy Storage* **2024**, *77*, 110058.
[28] P. Zhang, G. Zhang, Y. Liu, Y. Fan, X. Shi, Y. Dai, S. Gong, J. Hou, J. Ma, Y. Huang, R. Zhang, *J. Colloid Interface Sci.* **2024**, *654*, 1405–1416.
[29] Y. Zhou, M. Sun, M. Cao, Y. Zeng, M. Su, A. Dou, X. Hou, Y. Liu, *J. Colloid Interface Sci.* **2024**, *657*, 472–481.
[30] Y. Feng, Q. Huang, Z. Ding, L. Zhang, C. Liang, X. Luo, P. Gao, L. Zhou, W. Wei, *Electrochim. Acta* **2022**, *433*, 141253.
[31] L. Zhang, C. Guan, J. Zheng, H. Li, S. Li, S. Li, Y. Lai, Z. Zhang, *Sci. Bull.* **2023**, *68*, 180–191.
[32] M. Bianchini, J. Wang, R. J. Clément, B. Ouyang, P. Xiao, D. Kitchaev, T. Shi, Y. Zhang, Y. Wang, H. Kim, M. Zhang, J. Bai, F. Wang, W. Sun, G. Ceder, *Nat. Mater.* **2020**, *19*, 1088–1095.
[33] R. Liu, W. Huang, J. Liu, Y. Li, J. Wang, Q. Liu, L. Ma, G. Kwon, S. N. Ehrlich, Y. Wu, T. Liu, K. Amine, H. Li, *Adv. Mater.* **2024**, *36*, 2401048.
[34] C. Chen, W. Huang, Y. Li, M. Zhang, K. Nie, J. Wang, W. Zhao, R. Qi, C. Zuo, Z. Li, H. Yi, F. Pan, *Nano Energy* **2021**, *90*, 106504.
[35] S.-J. Park, J. Lee, I.-H. Ko, S. Koo, S. H. Song, C. Koo, G.-H. Yoon, T.-Y. Jeon, H. Kim, D. Kim, S.-H. Yu, *Energy Storage Mater.* **2021**, *42*, 97–108.
[36] S. Komaba, N. Yabuuchi, T. Nakayama, A. Ogata, T. Ishikawa, I. Nakai, *Inorg. Chem.* **2012**, *51*, 6211–6220.
[37] P.-F. Wang, Y. You, Y.-X. Yin, Y.-S. Wang, L.-J. Wan, L. Gu, Y.-G. Guo, *Angew. Chem. Int. Ed.* **2016**, *55*, 7445–7449.
[38] L. Yu, X. He, B. Peng, F. Wang, N. Ahmad, Y. Shen, X. Ma, Z. Tao, J. Liang, Z. Jiang, Z. Diao, B. He, Y. Xie, B. Qing, C. Wang, Y. Wang, G. Zhang, *Adv. Funct. Mater.* **2024**, *34*, 2406771.
[39] J. Mu, T. Cai, W. Dong, C. Zhou, Z. Han, F. Huang, *Chem. Eng. J.* **2023**, *471*, 144403.
[40] J. Zhai, H. Ji, W. Ji, R. Wang, Z. Huang, T. Yang, C. Wang, T. Zhang, Z. Chen, W. Zhao, A. Tayal, L. Jin, J. Wang, Y. Xiao, *Mater. Today Energy* **2022**, *29*, 101106.
[41] J. E. Wang, H. Kim, Y. H. Jung, D. K. Kim, D. J. Kim, *Small* **2021**, *17*, 2100146.
[42] S. Jia, M. Abdolhosseini, C. Liu, A. Jonderian, Y. Li, H. Kwak, S. Kumakura, J. M. Sieffert, M. Eisnor, E. McCalla, *Adv. Energy Sustain. Res.* **2024**, *5*, 2400051.
[43] L. Mu, X. Feng, R. Kou, Y. Zhang, H. Guo, C. Tian, C.-J. Sun, X.-W. Du, D. Nordlund, H. L. Xin, F. Lin, *Adv. Energy Mater.* **2018**, *8*, 1801975.
[44] N. A. Katcho, J. Carrasco, D. Saurel, E. Gonzalo, M. Han, F. Aguesse, T. Rojo, *Adv. Energy Mater.* **2017**, *7*, 1601477.
[45] P. Zhou, Z. Che, J. Liu, J. Zhou, X. Wu, J. Weng, J. Zhao, H. Cao, J. Zhou, F. Cheng, *Energy Storage Mater.* **2023**, *57*, 618–627.
[46] X. Liang, Y.-K. Sun, *Adv. Funct. Mater.* **2022**, *32*, 2206154.
[47] J. Liu, J. Zhou, Z. Zhao, Z. Che, J. Weng, X. Wu, X. Tang, P. Zhou, J. Zhou, S. Zhuo, *J. Power Sources* **2023**, *560*, 232686.

© 2025 The Authors. ChemElectroChem published by Wiley-VCH GmbH

21960216, 2025, 7, Downloaded from https://chemistry-europe.onlinelibrary.wiley.com/doi/10.1002/celc.202400657 by Ewha Womans University Library, Wiley Online Library on [10/08/2025]. See the Terms and Conditions (https://onlinelibrary.wiley.com/terms-and-conditions) on Wiley Online Library for rules of use; OA articles are governed by the applicable Creative Commons License

[48] Y. Wang, M. Yan, K. Xu, Y.-X. Chang, J. Guo, Q. Wang, B. Wang, D. Wang, Y.-X. Yin, S. Xu, *Inorg. Chem. Front.* **2022**, *9*, 5231–5239.
[49] L. Li, Q. Wu, S. Zhang, S. Li, Y. Cao, H. Zhang, Z. Li, *ACS Appl. Energy Mater.* **2023**, *6*, 9347–9355.
[50] W. Choi, H.-C. Shin, J. M. Kim, J.-Y. Choi, W.-S. Yoon, *J. Electrochem. Sci. Technol.* **2020**, *11*, 1–13.
[51] Y. Xiao, H.-R. Wang, H.-Y. Hu, Y.-F. Zhu, S. Li, J.-Y. Li, X.-W. Wu, S.-L. Chou, *Adv. Mater.* **2022**, *34*, 2202695.
[52] D. Zhou, C. Zeng, D. Ling, T. Wang, Z. Gao, J. Li, L. Tian, Y. Wang, W. Huang, *J. Alloys Compd.* **2023**, *931*, 167567.
[53] E. Lee, J. Lu, Y. Ren, X. Luo, X. Zhang, J. Wen, D. Miller, A. DeWahl, S. Hackney, B. Key, D. Kim, M. D. Slater, C. S. Johnson, *Adv. Energy Mater.* **2014**, *4*, 1400458.
[54] D. Zhou, W. Huang, X. Lv, F. Zhao, *J. Power Sources* **2019**, *421*, 147–155.
[55] Z.-C. Jian, Y.-F. Liu, Y.-F. Zhu, J.-Y. Li, H.-Y. Hu, J. Wang, L.-Y. Kong, X.-B. Jia, H.-X. Liu, J.-X. Guo, M.-Y. Li, Y.-S. Xu, J.-F. Mao, S.-L. Zhang, Y. Su, S.-X. Dou, S.-L. Chou, Y. Xiao, *Nano Energy* **2024**, *125*, 109528.
[56] S. P. Vanam, P. Barpanda, *Electrochim. Acta* **2022**, *431*, 141122.
[57] Q. Huang, S. Xu, L. Xiao, P. He, J. Liu, Y. Yang, P. Wang, B. Huang, W. Wei, *Inorg. Chem.* **2018**, *57*, 15584–15591.
[58] Y.-N. Zhou, P.-F. Wang, Y.-B. Niu, Q. Li, X. Yu, Y.-X. Yin, S. Xu, Y.-G. Guo, *Nano Energy* **2019**, *55*, 143–150.
[59] F. Hong, X. Zhou, X. Liu, G. Feng, H. Zhang, W. Fan, B. Zhang, M. Zuo, W. Xing, P. Zhang, H. Yan, W. Xiang, *J. Energy Chem.* **2024**, *91*, 501–511.
[60] H. N. Vasavan, M. Badole, S. Saxena, V. Srihari, A. K. Das, P. Gami, S. Deswal, P. Kumar, S. Kumar, *J. Energy Storage* **2023**, *74*, 109428.
[61] Q. Huang, J. Liu, L. Zhang, S. Xu, L. Chen, P. Wang, D. G. Ivey, W. Wei, *Nano Energy* **2018**, *44*, 336–344.
[62] H. N. Vasavan, M. Badole, S. Saxena, V. Srihari, A. K. Das, P. Gami, S. Deswal, P. Kumar, S. Kumar, *Mater. Today Energy* **2023**, *37*, 101380.
[63] S. Guo, Y. Sun, J. Yi, K. Zhu, P. Liu, Y. Zhu, G. Zhu, M. Chen, M. Ishida, H. Zhou, *NPG Asia Mater.* **2016**, *8*, e266–e266.
[64] S.-Y. Lee, H. Kweon, S. Lee, M. Cho, H. Ahn, J. Ahn, B. Ku, M. Choi, H.-G. Jung, D. O. Shin, J. Kim, *Adv. Energy Mater.* **2024**, *14*, 2402412.
[65] Z. Yan, L. Tang, Y. Huang, W. Hua, Y. Wang, R. Liu, Q. Gu, S. Indris, S.-L. Chou, Y. Huang, M. Wu, S.-X. Dou, *Angew. Chem. Int. Ed.* **2019**, *58*, 1412–1416.
[66] H. Ren, X.-W. Gao, D. Yong, Z. Liu, X. Wang, G. Gao, H. Chen, Q. Gu, W.-B. Luo, *Chem. Eng. J.* **2024**, *494*, 152787.
[67] S.-Y. Zhang, Y.-J. Guo, Y.-N. Zhou, X.-D. Zhang, Y.-B. Niu, E.-H. Wang, L.-B. Huang, P.-F. An, J. Zhang, X.-A. Yang, Y.-X. Yin, S. Xu, Y.-G. Guo, *Small* **2021**, *17*, 2007236.
[68] H.-R. Yao, P.-F. Wang, Y. Gong, J. Zhang, X. Yu, L. Gu, C. OuYang, Y.-X. Yin, E. Hu, X.-Q. Yang, E. Stavitski, Y.-G. Guo, L.-J. Wan, *J. Am. Chem. Soc.* **2017**, *139*, 8440–8443.
[69] P.-F. Wang, Y. You, Y.-X. Yin, Y.-G. Guo, *J. Mater. Chem. A* **2016**, *4*, 17660–17664.
[70] H. Liu, J. Xu, C. Ma, Y. S. Meng, *Chem. Commun.* **2015**, *51*, 4693–4696.
[71] T. Hwang, J.-H. Lee, S. H. Choi, R.-G. Oh, D. Kim, M. Cho, W. Cho, M.-S. Park, *ACS Appl. Mater. Interfaces* **2019**, *11*, 30894–30901.
[72] A. Ramesh, A. Tripathi, M. Bosman, S. Xi, P. Balaya, *Journal of J. Electroanal. Chem.* **2023**, *932*, 117222.
[73] H. V. S. R. M. Koppisetti, H. Rao, H. V. Ramasamy, H. R. Inta, S. Das, S. Kim, Y. Zhang, H. Wang, V. Mahalingam, V. G. Pol, *ACS Appl. Mater. Interfaces* **2023**, *15*, 32291–32300.
[74] Z. Liu, K. Jiang, S. Chu, J. Wu, H. Xu, X. Zhang, P. Wang, S. Guo, H. Zhou, *J. Mater. Chem. A* **2020**, *8*, 23820–23826.
[75] A. Kulka, C. Marino, K. Walczak, C. Borca, C. Bolli, P. Novák, C. Villevieille, *J. Mater. Chem. A* **2020**, *8*, 6022–6033.
[76] X. Ma, H. Chen, G. Ceder, *J. Electrochem. Soc.* **2011**, *158*, A1307.
[77] K. Kubota, M. Miyazaki, E. J. Kim, H. Yoshida, P. Barpanda, S. Komaba, *J. Mater. Chem. A* **2021**, *9*, 26810–26819.
[78] P.-F. Wang, H.-R. Yao, Y. You, Y.-G. Sun, Y.-X. Yin, Y.-G. Guo, *Nano Res.* **2018**, *11*, 3258–3271.
[79] B. Peng, Z.-H. Zhou, P. Xuan, J. Xu, L.-B. Ma, *Rare Met.* **2024**, *43*, 2093–2102.
[80] M. Liu, Z. Cheng, X. Zhu, H. Dong, T. Yan, L. Zhang, L. Zheng, H.-R. Yao, X.-Z. Wang, L. Yu, B. Xiao, Y. Xiao, P.-F. Wang, *Carbon Energy* **2024**, *6*, e565.
[81] C. Li, M. Li, G. Liu, H. Zhuo, Q. Li, H. Zhang, G. Pang, X. Yang, Z. Liao, K. Wang, D. Wang, B. Xiao, D. Geng, *ACS Appl. Mater. Interfaces* **2024**, *16*, 46216–46225.
[82] G. Liu, W. Xu, J. Wu, Y. Li, L. Chen, S. Li, Q. Ren, J. Wang, *J. Energy Chem.* **2023**, *83*, 53–61.
[83] Y. He, Q. Chen, W. Lai, *Solid State Ionics* **2023**, *399*, 116298.
[84] D. Wang, Y.-P. Deng, Y. Liu, Y. Jiang, B. Zhong, Z. Wu, X. Guo, Z. Chen, *Nano Energy* **2023**, *110*, 108340.
[85] D. Wang, H. Chen, X. Zheng, L. Qiu, J. Qu, Z. Wu, Y. Zhong, W. Xiang, B. Zhong, X. Guo, *ChemElectroChem* **2019**, *6*, 5155.
[86] S. Li, W. Zhou, F. Liu, C. Guan, X. Gao, Y. Zhang, R. Jin, Y. Lai, Z. Zhang, *Adv. Energy Mater.* **2024**, 2403955.
[87] Y. Yang, Q. Wang, J. Hou, J. Liu, T. Sun, M. Tang, C.-T. Chen, C.-Y. Kuo, Z. Hu, T. Zheng, G. Yan, J. Ma, *Angew. Chem. Int. Ed.* **2024**, *63*, e202411059.
[88] X. Zhu, H. Dong, Y. Liu, Y.-H. Feng, Y. Tang, L. Yu, S.-W. Xu, G.-X. Wei, S. Sun, M. Liu, B. Xiao, R. Xu, Y. Xiao, S. Chou, P.-F. Wang, *ACS Nano* **2024**, *18*, 32003–32015.
[89] M. Schmidt, V. Mereacre, H. Geßwein, N. Bohn, S. Indris, J. R. Binder, *Adv. Energy Mater.* **2024**, *14*, 2301854.
[90] X. Liu, C. Yuan, X. Zheng, G. Cheng, H. Qian, B. Zheng, X. Lu, Y. Yang, Y. Zhu, Y. Xiang, *Adv. Mater.* **2024**, *36*, 2407519.
[91] Q. Wang, D. Zhou, C. Zhao, J. Wang, H. Guo, L. Wang, Z. Yao, D. Wong, G. Schuck, X. Bai, J. Lu, M. Wagemaker, *Nat. Sustain.* **2024**, *7*, 338–347.

Manuscript received: November 29, 2024
Revised manuscript received: January 31, 2025
Version of record online: February 18, 2025

© 2025 The Authors. ChemElectroChem published by Wiley-VCH GmbH

21960216, 2025, 7, Downloaded from https://chemistry-europe.onlinelibrary.wiley.com/doi/10.1002/celc.202400657 by Ewha Womans University Library, Wiley Online Library on [10/08/2025]. See the Terms and Conditions (https://onlinelibrary.wiley.com/terms-and-conditions) on Wiley Online Library for rules of use; OA articles are governed by the applicable Creative Commons License